



## Contributions of biomass-burning, urban, and biogenic emissions to the concentrations and light-absorbing properties of particulate matter in central Amazonia during the dry season

Suzane S. de Sá (1), Luciana V. Rizzo (2), Brett B. Palm<sup>a</sup> (3), Pedro Campuzano-Jost (3), Douglas A. Day (3), Lindsay D. Yee (4), Rebecca Wernis (5), Gabriel Isaacman-VanWertz<sup>b</sup> (4), Joel Brito<sup>c</sup> (6), Samara Carbone<sup>d</sup> (6), Yingjun J. Liu<sup>e</sup> (1), Arthur Sedlacek (7), Stephen Springston (7), Allen H. Goldstein (4), Henrique M. J. Barbosa (6), M. Lizabeth Alexander (8), Paulo Artaxo (6), Jose L. Jimenez (3), Scot T. Martin\* (1,9)

- (1) John A. Paulson School of Engineering and Applied Sciences, Harvard University, Cambridge, Massachusetts, USA
- (2) Department of Environmental Sciences, Universidade Federal de São Paulo, Diadema, São Paulo, Brazil
- (3) Department of Chemistry and Cooperative Institute for Research in Environmental Sciences, University of Colorado, Boulder, Colorado, USA
- (4) Department of Environmental Science, Policy, and Management, University of California, Berkeley, Berkeley, California, USA
- (5) Department of Civil and Environmental Engineering, University of California, Berkeley, Berkeley, California, USA
- (6) Institute of Physics, University of São Paulo, São Paulo, Brazil
- (7) Brookhaven National Laboratory, Upton, New York, USA
- (8) Environmental Molecular Sciences Laboratory, Pacific Northwest National Laboratory, Richland, Washington, USA
- (9) Department of Earth and Planetary Sciences, Harvard University, Cambridge, Massachusetts, USA

<sup>a</sup> Now at Department of Atmospheric Sciences, University of Washington, Seattle, USA

<sup>b</sup> Now at Department of Civil and Environmental Engineering, Virginia Tech, Blacksburg, Virginia, USA

<sup>c</sup> Now at IMT Lille Douai, Université Lille, SAGE, Lille, France

<sup>d</sup> Now at Agrarian Sciences Institute, Federal University of Uberlândia, Minas Gerais, Brazil

<sup>e</sup> Now at College of Environmental Science and Engineering, Peking University, Beijing, China

\*To Whom Correspondence Should be Addressed

*E-mail:* [scot\\_martin@harvard.edu](mailto:scot_martin@harvard.edu)

*https://martin.seas.harvard.edu/*



## 1 Abstract

2 Urbanization and deforestation have important impacts on atmospheric particulate matter  
3 (PM) over Amazonia. This study presents observations and analysis of submicron PM<sub>1</sub>  
4 concentration, composition, and optical properties in central Amazonia during the dry season.  
5 The focus is on delineating the anthropogenic impact on the observed quantities, especially as  
6 related to the organic PM<sub>1</sub>. The primary study site was located 70 km to the west of Manaus, a  
7 city of over two million people in Brazil. As part of the GoAmazon2014/5 experiment, datasets  
8 from a large suite of instrumentation were employed. A high-resolution time-of-flight aerosol  
9 mass spectrometer (AMS) provided data on PM<sub>1</sub> composition, and aethalometer measurements  
10 were used to derive the absorption coefficient  $b_{\text{abs,BrC}}$  of brown carbon (BrC) at 370 nm. The  
11 relationships of  $b_{\text{abs,BrC}}$  with AMS-measured quantities showed that the absorption was  
12 associated with less-oxidized, nitrogen-containing organic compounds. Atmospheric processing  
13 appeared to bleach the BrC components. The organic PM<sub>1</sub> was separated into different classes by  
14 positive-matrix factorization (PMF). Estimates of the effective mass absorption efficiency  
15 associated with each PMF factor were obtained. Biomass burning and urban emissions appeared  
16 to contribute at least 80% of  $b_{\text{abs,BrC}}$  while accounting for 30 to 40 % of the organic PM<sub>1</sub> mass  
17 concentration. In addition, a comparison of organic PM<sub>1</sub> composition between wet and dry  
18 seasons revealed that only a fraction of the nine-fold increase in mass concentration between the  
19 seasons was due to biomass burning. An eight-fold increase in biogenic secondary organic PM<sub>1</sub>  
20 was observed. A combination of decreased wet deposition and increased emissions and oxidant  
21 concentrations, as well as a positive feedback on larger mass concentrations are thought to play a  
22 role in the observed increases. Fuzzy c-means clustering identified three clusters to represent  
23 different pollution influences during the dry season, including “baseline” (dry season  
24 background, which includes biomass burning), “event” (increased influence of biomass burning  
25 and long-range transport of African volcanic emissions), and “urban” (Manaus influence on top



26 of the background). The baseline cluster was associated with a mean mass concentration of  $9 \pm 3$   
27  $\mu\text{g m}^{-3}$ . This concentration increased on average by  $3 \mu\text{g m}^{-3}$  for both the urban and the event  
28 clusters. The event cluster was characterized by remarkably high sulfate concentrations.  
29 Differences in the organic  $\text{PM}_{10}$  composition for the urban cluster compared to the other two  
30 clusters suggested a shift in oxidation pathways as well as an accelerated oxidation cycle due to  
31 urban emissions, in agreement with findings for the wet season.



## 32 1. Introduction

33 The Amazon basin has undergone significant urbanization and deforestation in the past  
34 decades (Davidson et al., 2012; Martin et al., 2017; van Marle et al., 2017). An understanding of  
35 how the composition of atmospheric particulate matter (PM) changes due to anthropogenic  
36 activities and how these changes affect PM optical properties is essential for quantifying the  
37 global anthropogenic radiative forcing (IPCC, 2013; Sena et al., 2013). Light absorption  
38 coefficients,  $b_{\text{abs}}$ , and their spectral dependence, commonly referred to as the Ångström  
39 absorption exponent,  $\alpha_{\text{abs}}$ , are needed for accurate interpretation of satellite-retrieved aerosol  
40 optical depth (AOD) for climate modeling. Estimates of the mass absorption efficiency  $E_{\text{abs}}$  for  
41 PM subcomponents are useful for models to estimate optical effects based on PM composition  
42 and mass concentrations (Laskin et al., 2015).

43 Organic material that can efficiently absorb radiation in the near-ultraviolet through the  
44 blue end of the visible spectrum, with decreasing absorption efficiency as wavelength increases,  
45 is termed “brown carbon” (BrC) (Pöschl, 2003; Andreae and Gelencsér, 2006; Laskin et al.,  
46 2015). By comparison, black carbon (BC) absorbs light efficiently throughout the visible  
47 spectrum. Although global climate models have typically treated organic PM as purely  
48 scattering, several studies have shown that brown carbon can contribute substantially to light  
49 absorption by PM, especially in regions affected by biomass burning and urban emissions  
50 (Andreae and Gelencsér, 2006; Ramanathan et al., 2007; Bond et al., 2011; Bahadur et al., 2012;  
51 Ma and Thompson, 2012; Feng et al., 2013). In addition to primary emissions of BrC, secondary  
52 production of BrC can occur from the oxidation of volatile organic compounds (VOCs) present  
53 in biomass smoke (Saleh et al., 2014) and from atmospheric multiphase reactions involving a  
54 wide range of precursor VOCs (Nozière et al., 2007; De Haan et al., 2009; Nguyen et al., 2012;



55 Lee et al., 2013; Lin et al., 2014; Powelson et al., 2014). The specific sources, chemical  
56 characteristics, and optical properties of BrC remain largely unconstrained.

57 Biomass burning and urban pollution can affect the concentrations, composition, and  
58 properties of atmospheric PM. In Amazonia, urban pollution is significant downwind of large  
59 cities such as Manaus, Brazil (Kuhn et al., 2010; Martin et al., 2017; Cirino et al., 2018; de Sá et  
60 al., 2018). Martin et al. (2017) reported increased concentrations of particles, nitrogen oxides,  
61 carbon monoxide, and hydroxyl radicals for in-plume compared to out-of-plume conditions  
62 downwind of Manaus. Liu et al. (2016) and de Sá et al. (2017) demonstrated that the Manaus  
63 pollution plume shifted the oxidation pathway of isoprene, thereby significantly affecting gas-  
64 and particle-phase compositions. de Sá et al., 2018 determined that the submicron PM mass  
65 concentration increased by up to three-fold for polluted compared to background conditions  
66 downwind of Manaus during the wet season.

67 Most biomass burning in Amazonia is related to human activities (Davidson et al., 2012;  
68 Artaxo et al., 2013; Aragão et al., 2014; van Marle et al., 2017). Among the main activities are  
69 the clearing of land and the burning of waste for several agricultural purposes as well as the  
70 burning of wood as fuel (Crutzen and Andreae, 1990; van Marle et al., 2017). Burning events are  
71 most frequent in the period of August through October, corresponding to the dry season (Setzer  
72 and Pereira, 1991; Artaxo et al., 2013; Martin et al., 2016). These activities can affect the  
73 biogeochemical cycles, atmospheric chemistry, precipitation, and climate throughout Amazonia  
74 (Crutzen and Andreae, 1990; Andreae et al., 2004; Lin et al., 2006). PM<sub>1</sub> mass concentrations  
75 typically increase by an order of magnitude between the wet and dry seasons in the Amazon,  
76 which has been commonly attributed to the increased biomass burning emissions (Artaxo et al.,  
77 1994; Holben et al., 1996; Martin et al., 2010b; Artaxo et al., 2013, and references therein).



78 Related increases in  $b_{\text{abs}}$  by one order of magnitude have also been attributed to biomass burning  
79 (Rizzo et al., 2011; Artaxo et al., 2013; Rizzo et al., 2013). Although black carbon is usually the  
80 main light-absorbing component for atmospheric particles smaller than  $1 \mu\text{m}$  ( $\text{PM}_{10}$ ), absorption  
81 by the organic BrC component of  $\text{PM}_{10}$  could also be significant (Rizzo et al., 2013; Wang et al.,  
82 2016; Saturno et al., 2017). Palm et al. (2018) showed that the formation potential of secondary  
83 organic  $\text{PM}_{10}$  increased by a factor of 1.7 in the dry season compared to the wet season, although  
84 biomass burning gases were not dominant precursors in either season. An understanding of the  
85 types and optical properties of organic components that may affect  $\text{PM}_{10}$  light absorption in the  
86 Amazon and elsewhere is still emerging (Laskin et al., 2015).

87 The study herein investigates the contributions of biomass burning, urban emissions, and  
88 biogenic emissions to the composition and optical properties of organic  $\text{PM}_{10}$  in central Amazonia  
89 during the dry season. Positive-matrix factorization (PMF) of organic mass spectra measured by  
90 an Aerosol Mass Spectrometer (AMS) was used to identify component classes of the organic  
91  $\text{PM}_{10}$ . A Fuzzy c-means clustering analysis of pollution indicators was employed to identify  
92 different conditions at the measurement site, as influenced by biomass burning and urban  
93 emissions. Connections are made between the optical properties of organic  $\text{PM}_{10}$ , including  
94  $b_{\text{abs,BrC}}$  and  $E_{\text{abs}}$ , and its component classes. Taken together, these three pieces of analysis allow  
95 for insights into the changes in particle concentration, composition, and optical properties  
96 associated with the influences of biomass burning and urban pollution downwind of Manaus.

## 97 **2. Methodology**

### 98 **2.1 Research sites and measurements**

99 The primary site of this study was called “T3”, located 70 km to the west of Manaus,  
100 Brazil, in central Amazonia (Martin et al., 2016; inset of Figure 1a). The pollution plume



101 primarily passed westerly of Manaus in the dry season and was modeled to intercept the T3 site  
102 about 60% of the time (Martin et al., 2017). Analyses of observational datasets have labeled  
103 pollution episodes for at least 15 to 30% of the time (Thalman et al., 2017; Cirino et al., 2018).  
104 Auxiliary sites “T0a” and “T2” served as references for background and urban-polluted  
105 conditions, respectively, in relation to T3. The T0a site was located at the Amazon Tall Tower  
106 Observatory (Andreae et al., 2015), about 150 km to the northeast of Manaus, and the air masses  
107 were typically upwind of the urban region without the influence of Manaus pollution. The T2 site  
108 was located 8 km to the west of Manaus, directly downwind of the city, and air masses were  
109 therefore typically heavily polluted at this site. During the dry season, the three sites were also  
110 affected by both nearby and long-range transported biomass burning emissions. The study period  
111 from August 15 to October 15, 2014, corresponded to the second Intensive Operating Period  
112 (IOP2) of the GoAmazon2014/5 experiment (Martin et al., 2016).

113 At the T3 site, mass concentrations of non-refractory PM<sub>1</sub> components (organic, sulfate,  
114 ammonium, nitrate, and chloride) were measured by a High-Resolution Time-of-Flight Aerosol  
115 Mass Spectrometer (AMS; DeCarlo et al., 2006; Sueper et al., 2018). A detailed description of  
116 operation was provided in de Sá et al. (2017). In brief, the AMS was deployed inside a  
117 temperature-controlled research container, and ambient data were collected every other 4 min.  
118 Data analysis was performed using *SQUIRREL* (1.56D) and *PIKA* (1.14G) of the AMS software  
119 suite (DeCarlo et al., 2006). The mean composition-dependent collection efficiency was 0.51  
120 (Section S1; Figure S1) (Middlebrook et al., 2012). Organic and inorganic nitrate concentrations  
121 were estimated from the AMS measurements based on the ratio of the signal intensity of NO<sub>2</sub><sup>+</sup> to  
122 that of NO<sup>+</sup> (Supplementary Material, Section S1, Figure S2) (Fry et al., 2009; Farmer et al.,  
123 2010; Fry et al., 2013). Sulfate measured by the AMS includes contributions from organo-



124 sulfates (Farmer et al., 2010; Glasius et al., 2018). The oxygen-to-carbon (O:C) and hydrogen-to-  
125 carbon (H:C) ratios of the organic PM<sub>1</sub> were calculated following the methods of Canagaratna et  
126 al. (2015).

127         Several other instruments complemented the AMS measurements. Gas- and particle-  
128 phase semi-volatile tracers were obtained by a Semi-Volatile Thermal Desorption Aerosol Gas  
129 Chromatograph (SV-TAG) (Isaacman-VanWertz et al., 2016; Yee et al., 2018), and VOCs were  
130 obtained by a Proton-Transfer-Reaction Time-of-Flight Mass Spectrometer (PTR-ToF-MS) (Liu  
131 et al., 2016). In addition, measurements of NO<sub>y</sub>, O<sub>3</sub>, particle number, and CO concentrations  
132 were employed in the analyses (Martin et al., 2016). Refractory black carbon (rBC)  
133 concentrations were measured by a Single Particle Soot Photometer (SP2). Meteorological  
134 variables, including temperature, relative humidity, and solar irradiance were also measured.  
135 Particle absorption coefficients  $b_{\text{abs}}(\lambda)$  were obtained by a seven-wavelength aethalometer (370,  
136 430, 470, 520, 565, 700, and 880 nm; Magee Scientific, model AE-31) following the methods  
137 and corrections of Rizzo et al., 2011. Additional measurements of non-refractory particle  
138 composition and concentration from the T0a and T2 sites were made by an Aerosol Chemical  
139 Speciation Monitor (ACSM) at each site (Ng et al., 2011; Andreae et al., 2015; Martin et al.,  
140 2016).

141         Air-mass backtrajectories were estimated using HYSPLIT4 (Draxler and Hess, 1998).  
142 Simulations started at 100 m above T3 and were calculated for every 12 min up to two days back  
143 in time. Input meteorological data on a grid of 0.5° × 0.5° were obtained from the Global Data  
144 Assimilation System (GDAS). Precipitation along the trajectories was based on data sets of the  
145 S-band radar of the System for Amazon Protection (SIPAM) in Manaus (Machado et al., 2014).





146 Additional information on the backtrajectory calculations and on the radar were described in de  
147 Sá et al. (2018).

## 148 2.2 Brown carbon light absorption

149 The analysis partitioned the total absorption  $b_{\text{abs}}(\lambda)$  measured by the aethalometer  
150 between BrC and BC contributions, as follows:

$$151 \quad b_{\text{abs}} = b_{\text{abs,BrC}} + b_{\text{abs,BC}} \quad (1)$$

152 The dependence on wavelength was expressed by the absorption Ångström exponent  $\mathring{a}_{\text{abs}}$ , as  
153 follows:

$$154 \quad \mathring{a}_{\text{abs}}(\lambda_1, \lambda_2) = - \frac{\log_{10}[b_{\text{abs}}(\lambda_1)/b_{\text{abs}}(\lambda_2)]}{\log_{10}(\lambda_1/\lambda_2)} \quad (2)$$

155 For the characterization of BrC absorption, the value of  $\mathring{a}_{\text{abs,BrC}}$  at 370 nm was sought. To  
156 calculate  $b_{\text{abs,BrC}}(370)$ , an assumption has to be made about the spectral dependency of BC light  
157 absorption. In this study,  $\mathring{a}_{\text{abs,BC}}$  was assumed to be wavelength-independent, and  $\mathring{a}_{\text{abs,BC}}(700,880)$   
158 was calculated for each sample based on  $b_{\text{abs}}$  at the wavelengths 700 and 880 nm (Eq. 2),  
159 assuming absorption to be insignificant for BrC and dominated by BC in this spectral range.  
160 Calculations of  $b_{\text{abs,BrC}}(370)$  using alternative treatments to retrieve  $\mathring{a}_{\text{abs,BC}}$  were also carried out.  
161 These treatments included the assumption that  $\mathring{a}_{\text{abs,BC}}$  is equal to 1.0 and wavelength-independent  
162 (e.g., Yang et al., 2009), or the assumption that  $\mathring{a}_{\text{abs,BC}}$  has a spectral dependency itself (Wang et  
163 al., 2016; Saturno et al., 2018a). The results from these different treatments correlated with one  
164 another ( $R^2 > 0.9$ ), and the  $b_{\text{abs,BrC}}$  estimate used in this study and detailed in the steps below  
165 represented a lower bound among the differing assumptions (Section S4).

166 For each point in time,  $b_{\text{abs,BrC}}(370)$  was estimated by the following steps: (1)  $b_{\text{abs,BC}}(700)$   
167 =  $b_{\text{abs}}(700)$  and  $b_{\text{abs,BC}}(880) = b_{\text{abs}}(880)$  assuming that  $b_{\text{abs,BrC}} = 0$  at red wavelengths, (2)  
168  $\mathring{a}_{\text{abs,BC}}(700,880)$  was calculated from Equation 2 using  $b_{\text{abs,BC}}(700)$  and  $b_{\text{abs,BC}}(880)$ , (3)



169  $b_{\text{abs,BC}}(370)$  was calculated from Equation 2, using  $b_{\text{abs,BC}}(880)$  and  $\hat{a}_{\text{abs,BC}}(370,880) =$   
170  $\hat{a}_{\text{abs,BC}}(700,880)$  under the assumption that  $\hat{a}_{\text{abs,BC}}$  was independent of wavelength, and finally (4)  
171  $b_{\text{abs,BrC}}(370)$  was obtained by Equation 1 using  $b_{\text{abs,BC}}(370)$  and  $b_{\text{abs}}(370)$ . The value of  $b_{\text{abs,BrC}}$  at  
172 430 nm was also obtained by the same process. Based on  $b_{\text{abs,BC}}(370)$  and  $b_{\text{abs,BC}}(430)$ ,  
173  $\hat{a}_{\text{abs}}(370,430)$  was estimated. Hereafter,  $b_{\text{abs}}$  and  $b_{\text{abs,BrC}}$  refer to 370 nm, and  $\hat{a}_{\text{abs}}$  refers to the  
174 range of 370 to 430 nm.

175 The aethalometer, like other filter-based measurement schemes (e.g., PSAP, TAP, or  
176 MAAP), is prone to artifacts. These artifacts may originate from light scattering by the filter  
177 media itself, the influence of the filter media on the microphysical properties of the collected  
178 particle (e.g., potential change in hygroscopic particle size), and the impact of the multiple  
179 scattered photons on the measured optical extinction (e.g., enhanced particle absorption as  
180 discussed by Nakayama et al., 2010). While several correction schemes have been developed to  
181 address these artifacts, the individual schemes do not approach these problems in the same way,  
182 which may lead to different results among them (Weingartner et al., 2003; Schmid et al., 2006;  
183 Collaud Coen et al., 2010; Rizzo et al., 2011; Ammerlaan et al., 2017). For the present analysis,  
184 the correction scheme used was described by Rizzo et al., 2011. The potential impact of the  
185 different correction schemes on the analysis interpretation was not examined.

### 186 **3. Results and discussion**

#### 187 **3.1 Contributions of biomass burning and urban emissions to fine-mode PM**

##### 188 **3.1.1 Comparison of PM concentration and composition across sites**

189 A comparison between the T3 site and the upwind sites can provide a first-order estimate  
190 of the effects of Manaus urban pollution on  $\text{PM}_{10}$  concentration and composition (de Sá et al.,  
191 2018). During the dry season of 2014, organic compounds dominated the composition at T3,



192 contributing  $83 \pm 6\%$  (mean  $\pm$  one standard deviation) of the non-refractory  $\text{PM}_{10}$  (NR- $\text{PM}_{10}$ ),  
193 followed by sulfate ( $11 \pm 5\%$ ) (Figure 1a). Mean NR- $\text{PM}_{10}$  mass concentrations and relative  
194 compositions at T3 and at T0a and T2 are represented in Figure 1b for comparison. Organic  
195 material consistently constituted 80% to 85% of NR- $\text{PM}_{10}$  across all three sites. By comparison,  
196 the contribution of organic material to NR- $\text{PM}_{10}$  typically ranged from 70 to 80% during the wet  
197 season (de Sá et al., 2018).

198 The NR- $\text{PM}_{10}$  mass concentrations across the three sites differed slightly (Figure 1b, top  
199 panel). The mean concentration at the T0a site upwind of Manaus was  $10.5 \mu\text{g m}^{-3}$ . The mean  
200 concentrations at the T2 site just downwind of Manaus and at the T3 site further downwind were  
201  $12.5 \mu\text{g m}^{-3}$  and  $12.2 \mu\text{g m}^{-3}$ , respectively, representing an increase of about 20% relative to the  
202 upwind site. By comparison, increases of 200 to 300% relative to the upwind site were observed  
203 during the wet season (de Sá et al., 2018). In absolute mass concentration, however, the  
204 difference between upwind and downwind sites of 1 to  $2 \mu\text{g m}^{-3}$  was similar between seasons,  
205 suggesting contributions from urban pollution in the same order of magnitude in both seasons.  
206 The larger percent increase for the wet season is explained by background concentrations of  $1 \mu\text{g}$   
207  $\text{m}^{-3}$  which are an order of magnitude lower compared to the dry season.

208 The time series of organic and sulfate mass concentrations across the three sites were  
209 highly correlated across the two months (Figure 2). The T0a and T3 sites were separated by 215  
210 km. This result shows that sources and processes of  $\text{PM}_{10}$  production at a regional scale were  
211 important during the dry season. The figure also shows that for timescales of less than a day the  
212 sites were less correlated. The large spikes in organic mass concentrations observed at T3 but  
213 generally smaller at T2 and absent at T0a could be explained by episodic fires along the  
214 Solimões River, especially during nighttime (Figure 3).



215 In addition to the widespread and frequent occurrence of fires in the Amazon basin  
216 during the dry season (Figure 3), meteorological conditions may also favor a regional reach of  
217 events (Section S3). For example, high organic concentrations were observed during the period  
218 of August 17 to 23. During that week, widespread biomass burning activity in the basin (beyond  
219 the scale of Figure 3) in conjunction with a lack of precipitation events, clear skies, and  
220 temperatures of 35 °C during daytime allowed for intense photochemical activity and buildup of  
221 PM<sub>1</sub>. There appeared to be an offset in PM<sub>1</sub> concentrations by 1 day between T0a and T3 during  
222 that time, which would be consistent with the transport across 215 km from T0a to T3 for typical  
223 easterlies averaging 3 m s<sup>-1</sup> over the course of a day. In short, a combination of regional-scale  
224 biomass burning activity and meteorological conditions greatly influenced the mass  
225 concentration of PM<sub>1</sub> at the three sites.

226 The diel variability of organic and sulfate mass concentrations for the three sites is shown  
227 in Figure 4. Organic mass concentrations were slightly higher at the T2 and T3 sites compared to  
228 the T0a site, as expected. The variability was larger at the T2 and T3 sites, especially so at night.  
229 These two sites are closer to populated areas along the path of the Solimões River and thus are  
230 also closer to local biomass burning sources. Activities include burning of crops and trash in  
231 houses and farms as well burning of wood in brick kilns (Martin et al., 2016; Cirino et al., 2018).  
232 Stagnant air and a shallow boundary layer during the night might explain how variable biomass  
233 burning emissions lead to larger organic mass concentrations and variability at night compared to  
234 the day.

235 The influence of anthropogenic emissions on daytime chemistry is apparent in the diel  
236 trends of the sulfate mass concentrations. Sulfate concentrations had low variability throughout  
237 the day at T0a, indicating a prevalence of diffuse regional sources that had variations dampened



238 after many hours or days of transport. Possible sources include the atmospheric oxidation of  
239 biogenic emissions (DMS, H<sub>2</sub>S) from the upwind forest and ocean, as well as long-range  
240 transport of fossil fuel combustion emissions from cities in northeastern Brazil and of biomass  
241 burning and volcanic emissions from Africa (Andreae et al., 1990; Martin et al., 2010a; Saturno  
242 et al., 2018b.) Biomass burning can be an important source of sulfate and its precursors (Andreae  
243 and Merlet, 2001; Fiedler et al., 2011). For the T2 and T3 sites, sulfate concentrations increased  
244 in the morning hours and peaked in the afternoon. The Manaus sulfate source consists of the  
245 burning of heavy fuel oil for electricity production, refinery operations, and more diffuse traffic  
246 sources, and these emissions reach the T3 site in the afternoon, when OH levels are also the  
247 highest (de Sá et al., 2017). In addition, biomass burning emissions around T2 and T3 might also  
248 have contributed to the increase in sulfate concentrations during the afternoons.

### 249 **3.1.2 Comparison of PM concentration and composition across clusters for the T3 site**

250 A second approach to investigate the changes in concentrations and compositions of the  
251 PM with pollution influences employed a combination of positive-matrix factorization (PMF)  
252 and Fuzzy c-means (FCM) clustering. The PMF analysis was applied to the organic mass spectra  
253 to separate the organic PM<sub>1</sub> into representative component classes (section 3.1.2.1). The FCM  
254 clustering algorithm was applied to auxiliary measurements to identify times of urban and  
255 biomass burning influences at the T3 site (section 3.1.2.2). The results of the FCM analysis were  
256 crossed with the findings of the PMF analysis for further insights into pollution-related  
257 variability of PM concentration and composition (section 3.1.2.3).

#### 258 **3.1.2.1 Classification of organic PM by positive-matrix factorization**

259 The organic mass spectra recorded by the AMS at the T3 site were analyzed by PMF  
260 (Ulbrich et al., 2009). Details and diagnostics of the PMF analysis are presented in the



261 Supplementary Material (Section S1). Following the nomenclature used in de Sá et al. (2018),  
262 “mass spectrum” and “mass concentration” refer to the direct AMS measurements, while “factor  
263 profile” and “factor loading” are their counterpart mathematical products obtained from the  
264 PMF analysis. A six-factor solution was obtained, and the factor profiles, diel trends of the factor  
265 loadings, and the time series of the factor loadings and other related measurements are plotted in  
266 Figure 5. The correlations of factor loadings with co-located measurements of gas- and particle-  
267 phase species are presented in Figure 6.

268 The factors were interpreted considering the mass spectral characteristics of the factor  
269 profiles and the correlations between factor loading and mass concentrations of co-located  
270 measurements. Three resolved factors interpreted as secondary production and processing  
271 closely matched the counterpart profiles of the wet season ( $R \geq 0.99$ ; Table 1) (de Sá et al.,  
272 2018). These three factors consisted of a more-oxidized oxygenated factor (“MO-OOA”), a less-  
273 oxidized oxygenated factor (“LO-OOA”), and an isoprene epoxydiols-derived factor (“IEPOX-  
274 SOA”). Temporal correlations with external tracers and oxidation characteristics were also  
275 similar to those of the wet season, corresponding to IOP1 (Figure 6; Table 1; de Sá et al., 2018).  
276 Although a hydrocarbon-like factor (“HOA”) was analogous to its counterpart in IOP1 ( $R =$   
277  $0.94$ ), it also had characteristics of an IOP1 anthropogenic-dominated factor (“ADOA”) tied to  
278 other urban sources including cooking. The HOA factor of IOP2 therefore represented a mix of  
279 the HOA and ADOA factors of IOP1, which could not be separated by PMF in IOP2 due to their  
280 lower relative contributions. The interpretation of the HOA, IEPOX-SOA, LO-OOA, and MO-  
281 OOA factors follows that of IOP1, as presented in de Sá et al. (2018). The following discussion  
282 focuses on the two biomass burning factors of IOP2.



283 A less-oxidized factor (“LO-BBOA”) and a more-oxidized factor (“MO-BBOA”) were  
284 resolved for IOP2. For IOP1, a single “BBOA” factor was resolved, and it accounted for 9% of  
285 the organic PM<sub>1</sub> mass concentration. For IOP2, there were enough differences in mass spectral  
286 features and temporal contributions, as well as larger overall contributions of biomass burning,  
287 that the PMF analysis identified two different factors. The MO-BBOA and LO-BBOA factors  
288 respectively accounted for 18% and 12% of the mean organic PM<sub>1</sub> mass concentration.  
289 Therefore, the relative contribution of biomass burning to organic PM<sub>1</sub> during the dry season was  
290 at least a factor of three higher compared to the wet season (a more detailed discussion is  
291 presented at the end of this section).

292 The LO-BBOA and MO-BBOA factor profiles had a distinct peak at nominal  $m/z$  60  
293 ( $C_2H_4O_2^+$ ) (Figure 5a). The fractional intensity  $f_{60}$  at  $m/z$  60 was larger for LO-BBOA (0.051)  
294 than for MO-BBOA (0.013). A peak at  $m/z$  73 ( $C_3H_5O_2^+$ ) was also present in both profiles,  
295 although its intensity was three to four times smaller than that at  $m/z$  60. The peaks at  $m/z$  60 and  
296  $m/z$  73 are attributed to fragments of levoglucosan and other anhydrous sugars that are produced  
297 by the pyrolysis of biomass (Schneider et al., 2006; Cubison et al., 2011). Accordingly, the  
298 loadings of both factors correlated with the concentrations of several biomass-burning tracers in  
299 the particle phase, including levoglucosan, vanillin, 4-nitrocatechol, syringol, mannosan,  
300 syringaldehyde, sinapaldehyde, and long-chain alkanolic acids ( $C_{20}$ ,  $C_{22}$ ,  $C_{24}$ ) and of tracers in the  
301 gas phase (acetonitrile) (Figure 6). The loadings also correlated with less-specific tracers,  
302 including CO concentration and particle number concentration. The Pearson- $R$  correlations were  
303 typically higher for the LO-BBOA factor than for the MO-BBOA factor.

304 The LO-BBOA profile had the greatest ratio of signal intensity of the  $C_2H_3O^+$  ion ( $m/z$   
305 43) to that of the  $CO_2^+$  ion ( $m/z$  44) compared to all other factors (Figure 5a). In comparison, the



306 MO-BBOA profile had a high intensity for the  $\text{CO}_2^+$  ion and a low intensity for the  $\text{C}_2\text{H}_3\text{O}^+$  ion.  
307 The MO-BBOA and LO-BBOA factors had O:C ratios of  $0.70 \pm 0.07$  and  $0.53 \pm 0.04$ ,  
308 respectively. In addition, the LO-BBOA factor loading had higher correlation with the estimated  
309 inorganic nitrate concentrations than with the total nitrate concentrations whereas the MO-  
310 BBOA factor did not (Figure 6; Supplementary Material, Section S1 describes the nitrate  
311 estimates). Taken together, these results point to a less-oxidized, higher-volatility character of  
312 the LO-BBOA factor and a more-oxidized, lower-volatility character of the MO-BBOA factor,  
313 both with biomass-burning characteristics (Jimenez et al., 2009; Cubison et al., 2011; Gilardoni  
314 et al., 2016; Zhou et al., 2017).

315 The extent of the biomass burning influence and atmospheric oxidation on the  
316 composition of organic  $\text{PM}_{10}$  can be visualized in a scatter plot of  $f_{44}$  and  $f_{60}$  (Figure 7a) (Cubison  
317 et al., 2011). A background  $f_{60}$  value of  $0.3\% \pm 0.06\%$  (vertical black dashed line) indicates a  
318 threshold for negligible or completely oxidized biomass-burning  $\text{PM}_{10}$ . Points in the lower right  
319 of the  $f_{44}$ - $f_{60}$  representation usually characterize  $\text{PM}_{10}$  tied to recent biomass burning emissions.  
320 For IOP1 (blue markers), all points lie on or close to the background value suggested by Cubison  
321 et al. (2011), indicating the absence of a strong influence from biomass burning. During the wet  
322 season, biomass burning was limited to local sources or to sources far enough away such as  
323 Africa that the  $\text{PM}_{10}$  was extensively oxidized by arrival in central Amazonia (de Sá et al., 2018).  
324 For IOP2 (red markers), the  $f_{60}$  values are greater for most observations, showing that for most  
325 times T3 was influenced to some extent by biomass burning (see Section 3.1.2.3). This finding is  
326 in line with the widespread occurrence of fires during the dry season (Figure 3). As suggested by  
327 the robust trend in Figure 7a, the  $f_{44}$  value increases and the  $f_{60}$  value decreases from the bottom  
328 right to the upper left as the organic  $\text{PM}_{10}$  emitted by biomass burning is oxidized in the





329 atmosphere. The  $f_{60}$  and  $f_{44}$  values of the LO-BBOA and MO-BBOA profiles, plotted as  
330 diamonds, lie on the linear trend.

331 The LO-BBOA factor of high  $f_{60}/f_{44}$  and low O:C thus appears associated with primary  
332 PM<sub>1</sub> emitted by biomass burning. The MO-BBOA factor, characterized by low  $f_{60}/f_{44}$  and high  
333 O:C, may represent a combination of primary PM<sub>1</sub> of higher oxygen content as well as secondary  
334 PM<sub>1</sub> tied to biomass burning in its early stages of atmospheric processing (Cubison et al., 2011;  
335 Gilardoni et al., 2016). These secondary pathways could include (i) the heterogeneous oxidation  
336 of primary PM<sub>1</sub>, such as that represented by the LO-BBOA factor, and (ii) the oxidation of gas-  
337 phase biomass-burning emissions or of species evaporated from primary PM<sub>1</sub>, followed by the  
338 condensation of the gas-phase products onto the PM<sub>1</sub>.

339 The LO-BBOA and MO-BBOA factor loadings had greater magnitude and variability at  
340 night compared to during day (Figure 5b). Their summed loading, represented as “BBOA<sub>T</sub>”,  
341 accounted for 40% and 13% of the organic PM<sub>1</sub> during night and day, respectively. Overall, they  
342 accounted for 30% of the organic PM<sub>1</sub>. This result reflects the importance of fire activity during  
343 all times of day and during the entirety of IOP2 (Figure 3). The surface concentrations were  
344 lower during the day because biomass burning emissions are diluted with the development of the  
345 planetary boundary layer (PBL) and with the increased wind speeds as compared to the stagnant  
346 air and shallower PBL at night. The occurrence of significant dilution indicates that the emission  
347 sources were at least in part within a day of transport, meaning a distance on the order of a few  
348 hundred kilometers. The fractional contribution of the MO-BBOA factor to BBOA<sub>T</sub> shifted from  
349 0.7 to 0.5 from day to night, while that of LO-BBOA correspondingly shifted from 0.3 to 0.5  
350 (Figure 7b). This result is consistent with an additional secondary contribution to the MO-BBOA



351 loading during daytime, including from LO-BBOA oxidation and possibly tied to photochemical  
352 processing, on top of a primary source from biomass burning.

353         Although the footprint of biomass burning is geographically more widespread throughout  
354 the basin compared to the urban footprint of nearby Manaus, fire incidence and large-scale  
355 emissions have historically concentrated in a region known as the arc of deforestation along the  
356 southern rim of the forest (Fuzzi et al., 2007; Artaxo et al., 2013). Several campaigns have  
357 focused on the effects of biomass burning during the dry season at locations that are highly  
358 affected by fires, usually in the states of Rondônia or Mato Grosso, within the arc of  
359 deforestation (SCAR-B, Kaufman et al., 1998; LBA-SMOCC, Fuzzi et al., 2007; LBA-  
360 EUSTACH, Andreae et al., 2002; TROFEE, Yokelson et al., 2007; SAMBBA, Morgan et al.,  
361 2013). At a ground site in Porto Velho, Rondônia, a PMF analysis of ACSM data showed that  
362 70% of the organic PM<sub>1</sub> could be attributed to biomass burning (Brito et al., 2014). Compared to  
363 the present study, in which at least 30% of the organic PM<sub>1</sub> can be directly attributed to biomass  
364 burning, the contributions of fires to PM<sub>1</sub> in the arc of deforestation region are considerably  
365 larger.

366         The combined contribution of 30% by MO-BBOA and LO-BBOA at T3 represents a  
367 lower bound of biomass burning influence because more-oxidized material from biomass  
368 burning could be accounted for by the MO-OOA factor. In the limiting assumption that all MO-  
369 OOA loadings originated from BBOA loadings, an upper limit of 50% can be established for the  
370 mean contribution of biomass burning to organic PM<sub>1</sub> concentrations at T3. Considering that all  
371 organic PM<sub>1</sub> components have been observed to age into MO-OOA at similar rates (Jimenez et  
372 al., 2009), a more likely estimate of 38% can be derived by assuming that all factors contribute to  
373 MO-OOA proportionally to their ambient concentrations.



374 An important implication of these results, together with those of the wet season, is that  
375 although  $PM_{10}$  concentrations increase on average by a factor of 8.5 between seasons, not all of  
376 the increase is due to biomass burning, which has been a common assumption in previous studies  
377 (Artaxo et al., 1994; Holben et al., 1996; Echalar et al., 1998; Maenhaut et al., 1999; Andreae et  
378 al., 2002; Artaxo et al., 2002; Mace et al., 2003; Martin et al., 2010b; Artaxo et al., 2013; Rizzo  
379 et al., 2013; Brito et al., 2014; Pöhlker et al., 2016). In absolute mass concentrations, the  
380 contribution from biomass burning increased from  $0.12 \mu\text{g m}^{-3}$  in the wet season to  $3.4 \mu\text{g m}^{-3}$  in  
381 the dry season, which represents a 30-fold increase. This result corresponds to a change in  
382 percentage contribution to organic  $PM_{10}$  from 9% to 30% (not counting with the mass presumably  
383 present in MO-OOA). Nevertheless, the contribution from secondary biogenic sources (and their  
384 anthropogenically affected processes), as represented by the LO-OOA and IEPOX-SOA factors,  
385 also increased by around 8-fold from  $0.6 \mu\text{g m}^{-3}$  to  $4.8 \mu\text{g m}^{-3}$ . In absolute terms, this mass  
386 increase (of  $4.2 \mu\text{g m}^{-3}$ ) is comparable to the one associated with biomass burning ( $3.3 \mu\text{g m}^{-3}$ ).  
387 Because the 8-fold mass increase of LO-OOA and IEPOX-SOA was similar to the 8.5-fold  
388 increase in total organic  $PM_{10}$ , these factors show a similar mass percentage contribution of 42%  
389 to organic  $PM_{10}$  for both seasons. The MO-OOA factor loadings increased by 6-fold from  $0.4 \mu\text{g}$   
390  $\text{m}^{-3}$  to  $2.3 \mu\text{g m}^{-3}$ . Because this relative increase was smaller than that of the total organic  $PM_{10}$ ,  
391 the MO-OOA factor had a decrease from 30% to 20% of contribution to organic  $PM_{10}$ . The  
392 contribution from urban sources, as represented by the HOA and ADOA factors, increased by  
393 three-fold between seasons, from  $0.24 \mu\text{g m}^{-3}$  to  $0.76 \mu\text{g m}^{-3}$ , representing a decrease in mass  
394 percentage contribution from 18% to 7%.

395 Therefore, reasons other than increased biomass burning in the dry season must have  
396 played a role in increasing organic  $PM_{10}$  concentrations. One aspect is that BVOC emissions are



397 typically higher in the dry season (Yáñez-Serrano et al., 2015; Alves et al., 2016), which might  
398 partly explain the increases in LO-OOA, IEPOX-SOA, and MO-OOA factors. In addition, the  
399 directly-measured biogenic (total) secondary organic PM<sub>1</sub> formation potential of ambient air  
400 increased by a factor of 2.4 (1.7) between seasons (Palm et al., 2018). Increased organic mass  
401 available for partitioning may account for another factor of 2 (Palm et al., 2018). As a  
402 consequence of increased PM<sub>1</sub> mass concentrations, the lifetime of semi-volatile gases may also  
403 be increased, since lifetime against dry deposition is much larger for particles than for gases  
404 (Knote et al., 2015). Increased oxidant levels during the dry season could also be a contributing  
405 factor (Rummel et al., 2007; Artaxo et al., 2013; Andreae et al., 2015; Yáñez-Serrano et al.,  
406 2015; Fuentes et al., 2016). Importantly, the mass concentrations of sulfate and ammonium also  
407 increased by six-fold between seasons (Figure S10), indicating that atmospheric physical  
408 processes governing particle mass concentrations possibly played an important role. In this  
409 context, reduced wet deposition due to reduced convection in the dry season may be another  
410 appreciable contributor to the organic PM<sub>1</sub> increases (Machado et al., 2004; Nunes et al., 2016  
411 Chakraborty et al., 2018).

### 412 3.1.2.2 Cluster Analysis

413 The time series of the afternoon concentrations of particle number, NO<sub>y</sub>, ozone, rBC,  
414 carbon monoxide, and sulfate were analyzed by Fuzzy c-means clustering at the time resolution  
415 of the AMS measurements. The algorithm attributed degrees of cluster membership to each data  
416 point based on similarity in the sets of input concentrations (Section S2). The scope was  
417 restricted to data sets for which ten-hour air mass back trajectories did not intersect precipitation.  
418 The scope also excluded data sets tied to the lowest 10% of solar irradiance averaged over the  
419 previous 4 h at T3 (Supplementary Material, Section S2). This approach aimed to capture fair-



420 weather conditions and thereby minimize the role of otherwise confounding processes that  
421 influence mass concentrations, such as boundary layer dynamics and wet deposition.

422 Three clusters, labeled “baseline,” “event,” and “urban,” were identified based on a  
423 combination of minimization of the FCM objective function and an assessment of  
424 meaningfulness of the resolved set of clusters. Illustrative examples of the obtained degrees of  
425 membership (0 to 1) are plotted in Figure 8a for several time windows. The concentrations of the  
426 input and additional species are plotted in Figures 8b and 8c. The PMF results of section 3.1.2.1  
427 are plotted for comparison in Figure 8d. Air-mass backtrajectories are plotted in Figure 9 for  
428 time windows predominantly associated with only one cluster.

429 All three clusters reflected, albeit to different degrees, some influence of biomass  
430 burning. For the wet season, de Sá et al. (2018) identified clusters representing background  
431 conditions, which were characterized by low concentrations of particle number, NO<sub>y</sub>, and O<sub>3</sub>. For  
432 the dry season, no similar cluster was identified. As shown in Figure 3, there were fires in the  
433 region at all times (cf. Martin et al., 2017).

434 The baseline cluster had the lowest concentrations of pollutant indicators, representing  
435 influences of far-field biomass burning on top of natural (i.e., biogenic) emissions and  
436 atmospheric processing. The cluster centroid corresponded to 1.3 ppb NO<sub>y</sub>, 30 ppb ozone, and  
437 2000 particles cm<sup>-3</sup> (Table S1). Results for August 27, August 28, and September 9 illustrate  
438 these lower concentrations compared to the other days (Figure 8). The backtrajectories  
439 associated with the baseline cluster did not intersect the urban area of Manaus, especially the  
440 southern region of presumed higher emissions (Figure 9a; de Sá et al., 2018).

441 The event cluster referred to conditions of increased influence from biomass burning and  
442 long-range transport of volcanic emissions from Africa. The cluster corresponded to a 10-day



443 period from Sep 22 to Oct 1 in which biomass burning intensified in the surroundings of T3 as  
444 well as more broadly in the Amazon basin (Figures 3f and 3g). Coincidentally, plumes carrying  
445 emissions from the Nyamuragira-Nyiragongo volcanoes in Africa were also observed to reach  
446 central Amazonia during that time period, as demonstrated by Saturno et al. (2018b). This  
447 cluster was characterized by higher concentrations of all species in relation to the baseline cluster  
448 (Table S1). In particular, the sulfate concentrations ( $2.3 \mu\text{g m}^{-3}$  at the centroid) were the highest  
449 among the three clusters. Results for September 23, September 27, and September 28 illustrate  
450 these findings for T3, with sulfate concentrations reaching  $4 \mu\text{g m}^{-3}$  (Figure 8). This trend in  
451 sulfate concentrations was consistent across all three sites (Figure 2). The backtrajectories  
452 associated with the event cluster were variable, passing to the north, directly over, and to the  
453 south of Manaus, although always with an east component (Figure 9b). The long-range transport  
454 and increased regional fire count during the event period thus appeared more important in  
455 defining this cluster than did the directions of the backtrajectories in a smaller scale, making  
456 Manaus emissions of secondary importance.

457 The urban cluster had the highest centroid concentrations of  $\text{NO}_y$  (2.6 ppb), ozone (56.4  
458 ppb), and particle number ( $4600 \text{ cm}^{-3}$ ) among the three clusters (Table S1). It represented  
459 conditions for which both biomass burning and urban emissions were relevant, and these  
460 emissions may have interacted before reaching the T3 site. The results for August 24, September  
461 11, September 14, and October 8 illustrate the high pollutant concentrations (Figure 8). The  
462 backtrajectories associated with the urban cluster consistently passed over Manaus and, more  
463 specifically, over the southern region where human activities were more concentrated (Figure  
464 9c).



### 465 3.1.2.3 Comparison of PM<sub>1</sub> composition among clusters

466 Species mass concentrations and PMF factor loadings associated with the cluster  
467 centroids were determined (Section S2). The resulting organic, sulfate, ammonium, nitrate, and  
468 chloride mass concentrations associated with each cluster are represented in Figure 10a. The  
469 PMF factor loadings associated with each cluster are likewise represented in Figure 10b.

470 The summed NR-PM<sub>1</sub> mass concentrations for the centroids of the event and urban  
471 clusters were both 12.3  $\mu\text{g m}^{-3}$ . This concentration was 33% higher than that representing the  
472 baseline cluster (9.2  $\mu\text{g m}^{-3}$ ). This result thus agrees with that based on direct comparison of PM<sub>1</sub>  
473 mass concentrations between the T3 and the T0a sites (Section 3.1.1). Therefore, the overall  
474 effect of Manaus pollution was to add 1 to 3  $\mu\text{g m}^{-3}$  on top of the upwind concentrations.  
475 Increases in the organic mass concentration dominated the overall increase in PM<sub>1</sub> mass  
476 concentration because organic species dominated the composition for all three clusters. The  
477 increases in organic mass concentration for the event and urban clusters relative to the baseline  
478 cluster were 26% and 33%, respectively (Figure 10a).

479 Sulfate concentrations also increased relative to the baseline cluster, corresponding to  
480 65% for the event cluster and 31% for the urban cluster. This result indicates that strong biomass  
481 burning emissions reaching areas downwind of Manaus as well as long-range transport of  
482 volcanic emissions from as far away as Africa may increase sulfate concentrations in those areas  
483 beyond the sulfate values driven by the anthropogenic activities in the city. In other words, ,  
484 there were several other in-basin as well as out-of-basin sources of sulfate besides Manaus that  
485 could sustain relatively high sulfate concentrations (Chen et al., 2009; de Sá et al., 2017; Saturno  
486 et al., 2018b).



487           The relationship between clusters and PMF factors is represented in Figure 10b. All three  
488 clusters were associated with an organic PM<sub>1</sub> composition dominated by secondary production.  
489 The baseline cluster was largely dominated by the LO-OOA factor (40%). By comparison, the  
490 event cluster had significant increases in the LO-BBOA, MO-BBOA, and IEPOX-SOA factor  
491 loadings. The increase in LO-BBOA and MO-BBOA loadings (40%) can be associated with the  
492 increased contributions of primary and secondary particle components from biomass burning,  
493 respectively. The LO-BBOA factor had the highest loading (0.5 µg m<sup>-3</sup>) for the event cluster,  
494 consistent with the high incidence of fires during the period represented by this cluster. The  
495 increase of 65% in IEPOX-SOA loading can be explained by the disproportionally higher  
496 increase of 65% in the sulfate concentration (which favors higher IEPOX-SOA loadings),  
497 accompanied by the relatively moderate increase of 34% in NO<sub>y</sub> concentration, (which  
498 suppresses IEPOX-SOA loadings), leading to a net increase in IEPOX-SOA loadings (Table S1;  
499 de Sá et al., 2017).

500           The composition of the organic PM<sub>1</sub> associated with the urban cluster differed from that  
501 of the two other clusters, as indicated by the factor contributions (Figure 10). Compared to the  
502 baseline cluster, the loadings of all factors except IEPOX-SOA increased. An increase in HOA  
503 loading is consistent with emissions in the city, including from vehicles and power plants. An  
504 increase in the loadings associated with secondary processes, as represented by the MO-OOA,  
505 LO-OOA, and MO-BBOA factors, can be explained by the accelerated oxidation cycle in the  
506 plume. In brief, an increase in the concentrations of both precursors and oxidants provided by  
507 urban emissions accelerates the production of secondary PM<sub>1</sub> and thereby increases the PM<sub>1</sub>  
508 concentrations downwind of the city (Martin et al., 2017; de Sá et al., 2018).





509           The similarity in IEPOX-SOA factor loading for the baseline and the urban clusters may  
510 be explained by the following aspects. First, the lifetime of IEPOX-derived PM in the boundary  
511 layer is thought to be around 2 weeks (Hu et al., 2016). Therefore, a substantial fraction of this  
512 component observed at T3 will be formed upwind of the Manaus plume. Second, favored  
513 conditions for IEPOX production and uptake are low NO concentrations (i.e., HO<sub>2</sub>-dominant  
514 pathway for the ISOP<sub>OO</sub> radical) and high sulfate concentrations (de Sá et al., 2017). Sulfate  
515 concentrations increased by 31%, and NO<sub>y</sub> concentrations, used as an indicator for exposure of  
516 the airmass to NO concentrations, increased by 100% for the urban compared to the baseline  
517 cluster. These two changes work against one another with respect to IEPOX production and  
518 uptake. For the wet season, de Sá et al. (2017) reported that the IEPOX-SOA factor loading was  
519 more sensitive to changes in NO<sub>y</sub> concentration for 1 ppb and less. By comparison, NO<sub>y</sub>  
520 concentrations in the dry season were consistently greater than this value. Due to this lower  
521 sensitivity, large increases in NO<sub>y</sub> may not be tied to large decreases in IEPOX-SOA factor  
522 loading in the dry season. In sum, the opposite roles of sulfate and NO<sub>y</sub> concentrations can  
523 explain the net zero change in IEPOX-SOA factor loadings between baseline and urban clusters.  
524 Because all of the loadings for other factors increased, the fractional loading of IEPOX-SOA  
525 decreased from 26% to 15%.

## 526 **3.2 Contributions of biomass burning and urban emissions to brown carbon**

### 527 **3.2.1 Brown carbon light absorption**

528           The diel trends of  $b_{\text{abs}}$ ,  $b_{\text{abs,BrC}}$ ,  $b_{\text{abs,BrC}}/b_{\text{abs}}$ , and  $\hat{a}_{\text{abs}}$  are shown in Figure 11. Both  $b_{\text{abs}}$  and  
529  $b_{\text{abs,BrC}}$  were larger and had greater variability at night compared to day. The variability of the  
530 fractional contribution of BrC to the total absorption, represented by  $b_{\text{abs,BrC}}/b_{\text{abs}}$ , was smaller  
531 than the variability of its components  $b_{\text{abs}}$  and  $b_{\text{abs,BrC}}$  (i.e., Figure 11c compared to Figures 11a-



532 b). The absorptive contributions of BC and BrC thus co-varied to some extent, suggesting a  
533 partial overlap in sources, which is consistent with previous studies (Collier et al., 2016; Jen et  
534 al., 2018). Furthermore, the fractional contribution  $b_{\text{abs,BrC}}/b_{\text{abs}}$  increased from 0.2 in the day to  
535 0.4 at night. Compared to the diel trends of the six PMF factor loadings, the diel trends of the  
536 absorption properties were most similar to those of the MO-BBOA, LO-BBOA, and HOA  
537 factors (Figure 5b).

538 Figure 12 illustrates connections between  $b_{\text{abs,BrC}}$  and the organic PM<sub>1</sub> chemical  
539 composition. Brown-carbon light absorption decreases for increases in the O:C ratio (Figure  
540 12a). Conversely, light absorption increases for decreases in the concentration of nitrogen-  
541 containing species, as represented by the  $\text{C}_x\text{H}_y\text{O}_z\text{N}_p^+$  family (Figure 12b). In addition, light  
542 absorption increases as the fractional contribution of the  $\text{C}_x\text{H}_y\text{O}_z\text{N}_p^+$  family to organic PM<sub>1</sub>  
543 increases and that of the  $\text{C}_x\text{H}_y\text{O}_z^+$  family decreases (Figure S14). The diel trends of Figure 11 and  
544 the O:C ratios of Figure 12a support an association of brown-carbon light absorption with HOA  
545 and LO-BBOA factor loadings. These factors had the lowest O:C values (Table 1), and they are  
546 associated with recent urban and biomass burning emissions, which are typically important  
547 sources of brown carbon (Laskin et al., 2015, and references therein).

548 The decrease in  $b_{\text{abs,BrC}}$  as O:C increases suggests that the atmospheric processing of  
549 organic material bleaches the BrC components under the conditions of central Amazonia. This  
550 behavior has been observed in several laboratory studies: BrC species and thus their optical  
551 properties can be modified through atmospheric processing, which may involve reactions at the  
552 gas-particle interface, reactions in the aqueous phase of particle and cloud droplets, and  
553 photolysis driven by sunlight (Laskin et al., 2015; Zhao et al., 2015; Sumlin et al., 2017; Lee et  
554 al., 2014; Romonosky et al., 2015). In addition, Saleh et al. (2014) provided evidence that both



555 primary and secondary material from biomass burning may absorb light, and that the secondary  
556 component may be less absorptive than the primary component in the visible spectral range. Lin  
557 et al. (2016) found that the absorbance at 300 nm by biomass burning particles decayed with a  
558 half-life of approximately 16 h against photolysis under typical atmospheric conditions. Forrister  
559 et al. (2015) followed plumes from wildfires onboard an aircraft during the 2013 NASA  
560 SEAC4RS mission over the continental USA and estimated a half-life of 9 to 15 h for the decay  
561 of BrC light absorption in the plumes.

562 An important contribution of nitrogen-containing organic molecules to  $b_{\text{abs,BrC}}$  is  
563 suggested by the relationship in Figure 12b. The percent contribution of the  $\text{C}_x\text{H}_y\text{O}_z\text{N}_p^+$  family to  
564 each PMF factor profile is listed in Table 2 and is highest for the HOA and LO-BBOA factors.  
565 The correlations of factor loadings with the  $\text{C}_x\text{H}_y\text{O}_z\text{N}_p^+$  mass concentrations as well as with the  
566  $b_{\text{abs,BrC}}$  values are highest for these two factors ( $R > 0.8$  and  $R > 0.6$ , respectively) (Table 2). The  
567 correlations of the MO-BBOA factor loading with these two parameters are lower but still  
568 significant. By comparison, the corresponding correlations for the IEPOX-SOA, LO-OOA, and  
569 MO-OOA factor loadings are all lower than 0.5. These results further support that the HOA and  
570 LO-BBOA factors to a larger extent and the MO-BBOA factor to a lesser extent were tightly  
571 associated with nitrogen-containing, light-absorbing organic molecules.

572 In contrast to the  $\text{C}_x\text{H}_y\text{O}_z\text{N}_p^+$  family, the correlations between PMF factor loadings and  
573 mass concentrations of organic nitrates are low ( $R < 0.4$ , Table 2; Figure S12). For the HOA,  
574 LO-OOA, and MO-OOA factors associated with BrC light absorption, the correlations are small  
575 ( $R < 0.25$ ). The implication could be that the  $\text{C}_x\text{H}_y\text{O}_z\text{N}_p^+$  family is closely tied to  $\text{PM}_{10}$   
576 constituted by reduced nitrogen compounds and nitrogen-aromatic compounds. By comparison,



577 organic nitrates are more strongly tied to photochemical production of secondary PM<sub>1</sub> and  
578 represent more oxidized forms of nitrogen, including in aliphatic molecules.

579         Several studies have suggested that nitrogen-containing organic molecules are important  
580 absorbers in organic PM (Sun et al., 2007; Lin et al., 2016). Claeys et al. (2012) characterized  
581 humic-like substances (HULIS) present in PM collected during the biomass burning season in  
582 Amazonia and identified nitro-aromatic catechols and aromatic carboxylic acids among the main  
583 constituents. Nitrophenol derivatives have been identified as major BrC components in several  
584 other urban and rural locations worldwide (Kitanovski et al., 2012; Desyaterik et al., 2013; Kahnt  
585 et al., 2013; Mohr et al., 2013). Importantly, Lin et al., 2016 further verified that compounds that  
586 are usually interpreted as secondary, such as nitro-phenols and derivatives, can be produced in  
587 the heat-laden, VOC-rich, high-NO<sub>x</sub> conditions of the biomass burning process, being  
588 subsequently emitted as primary material. Furthermore, Yee et al. (2013) observed the quick  
589 conversion of guaiacol and syringol to nitro-guaiacol and nitro-syringol, respectively, in the  
590 presence of HONO even without heat or photo-oxidation. It is possible that BrC from other  
591 combustion sources could have similar characteristics based on this reasoning, helping to explain  
592 the association found in this study between BrC absorption and the LO-BBOA and HOA factors.  
593 Regarding the further atmospheric processing of these nitrogen-containing organic compounds,  
594 laboratory studies have shown that hydroxy radical oxidation of nitro-aromatic species in  
595 aqueous solutions leads to fragmentation into smaller organic acids (e.g., oxalic, glycolic,  
596 malonic, and isocyanic) or, in general, reduce the size of the conjugated molecular systems,  
597 leading to a decrease in light absorption at visible wavelengths (Sumlin et al., 2017; Hems and  
598 Abbatt, 2018). These findings may help to explain the bleaching of BrC as the material becomes  
599 more oxidized. In the context of the PMF factors, these smaller later-generation products may



600 then be associated with the MO-OOA factor or may partition to the gas phase depending on their  
601 volatility.

602 Scatter plots of  $\hat{a}_{\text{abs}}$  against markers of biomass burning are shown in Figure 13. The  
603 Pearson- $R$  correlations against  $\log_{10}(f_{60}/f_{44})$  and  $(\text{BBOA}_T/\text{organic PM}_1)$  are 0.87 and 0.75,  
604 respectively. The  $f_{60}/f_{44}$  ratio is a tracer for the influence of fresh biomass burning, and an  
605 association of  $\hat{a}_{\text{abs}}$  and with this quantity was also reported for Boulder, Colorado, USA (Lack et  
606 al., 2013). These relationships could be useful parameterizations to estimate  $\hat{a}_{\text{abs}}$  when optical  
607 measurements are not available but AMS / ACSM measurements are, at least during times of  
608 biomass burning influence in central Amazonia. Worldwide, observed values of  $\hat{a}_{\text{abs}}$  range from  
609  $<2$  to 11 for particles tied to biomass burning (Chakrabarty et al., 2010; Saleh et al., 2014). The  
610 value of  $\hat{a}_{\text{abs}}$  reached 6 for the highest observed values of  $(f_{60}/f_{44})$ . It approached 1.0 in the limit of  
611  $f_{60}/f_{44} < 0.02$ , which indicates little influence of proximate biomass burning (Figure 13a; cf.  
612 upper left of Figure 7a). Further observations elsewhere in the Amazon and on other regions are  
613 needed before the parameterizations suggested by Figure 13 between  $\hat{a}_{\text{abs}}$  and markers of  
614 biomass burning can be generalized with confidence.

### 615 3.2.2 Contribution of organic PM components to BrC absorption

616 Herein, advantage is taken of the representation of the organic PM in its subcomponents  
617 provided by the PMF factors to estimate a mass absorption efficiency for each of them. The  
618 absorption coefficient is the sum of the absorption coefficient of the  $n$  parts of the organic PM  
619 (“Org”):

$$620 \quad b_{\text{abs,BrC}} = b_{\text{abs,Org}_1} + b_{\text{abs,Org}_2} + \dots + b_{\text{abs,Org}_n} \quad (3)$$

621 The treatment assumes the absence of cross-interactions among the parts and holds for a single  
622 wavelength. The absorption coefficient  $b_{\text{abs},i}$  of part  $i$  is defined as follows:



623 
$$b_{\text{abs},i} = E_{\text{abs},i} \times C_i \quad (4)$$

624 where  $E_{\text{abs},i}$  is the mass absorption efficiency and  $C_i$  is the mass concentration of part  $i$ . Based on  
625 equations 3 and 4, the following model was constructed for  $b_{\text{abs,BrC}}$  by using the PMF factor  
626 loadings as a proxy for the mass concentrations of organic PM<sub>1</sub> components:

627 
$$b_{\text{abs,BrC}} = E_{\text{abs,MO-OOA}} G_{\text{MO-OOA}} + E_{\text{abs,LO-OOA}} G_{\text{LO-OOA}} + E_{\text{abs,IEPOX-SOA}} G_{\text{IEPOX-SOA}} +$$
  
$$+ E_{\text{abs,MO-BBOA}} G_{\text{MO-BBOA}} + E_{\text{abs,LO-BBOA}} G_{\text{LO-BBOA}} + E_{\text{abs,HOA}} G_{\text{HOA}} + B \quad (5)$$

628 where  $G_i$  correspond to loadings of factor  $i$ , and the unknowns are the mass absorption  
629 efficiencies  $E_{\text{abs},i}$  associated with each PMF factor. An intercept  $B$  was added to account for the  
630 variability not explained by the PMF factors. Other studies have also made use of multivariate  
631 linear regression to retrieve mass absorption efficiencies (Hand and Malm, 2007; Washenfelder et  
632 al., 2015).

633 Estimates of  $E_{\text{abs},i}$  were obtained using a constrained linear least-squares algorithm  
634 applied to Eq. 5, where the inputs were the observed  $b_{\text{abs,BrC}}$  and the factor loadings for each  
635 point in time during IOP2. The input data are represented in the scatter plots of  $G_i$  against  $b_{\text{abs,BrC}}$   
636 shown in Figures 14a to 14f. A non-negative constraint on the model coefficients  $E_{\text{abs},i}$  was  
637 included for physical meaning. The algorithm was applied in bootstrap with replacement of  
638 residuals for  $10^4$  runs, and convergence of the bootstrap results was checked by varying the  
639 number of samples. The resulting estimates of mean and standard error of  $E_{\text{abs}}$  for all PMF  
640 factors are listed in Table 3.

641 A scatter plot of the predicted  $b_{\text{abs,BrC,pred}}$  against the observed  $b_{\text{abs,BrC}}$  is shown in Figure  
642 14h. The model captured 66% of the variance in  $b_{\text{abs,BrC}}$ , and the PMF factor loadings can be  
643 considered good predictors of the BrC absorption under the study conditions. Physical factors not  
644 directly represented in this statistical model, such as the effects of mixing state, size distribution,



645 and so on for BrC absorption, either have low variability under the study conditions or  
646 alternatively have co-variability also captured in the PMF factor loadings.

647 The highest values of  $E_{\text{abs}}$  at 370 nm were associated with the HOA and LO-BBOA  
648 factors ( $2.04 \pm 0.14$  and  $1.50 \pm 0.07 \text{ m}^2 \text{ g}^{-1}$ , respectively). These results support the interpretation  
649 presented in the previous section about the association of the HOA and LO-BBOA factors with  
650 light absorption. As a point of comparison,  $E_{\text{abs}}$  of 2 to 3  $\text{m}^2 \text{ g}^{-1}$  at 300 nm was reported for  
651 HULIS extracts from PM<sub>2.5</sub> filter samples collected under biomass burning conditions during the  
652 Amazon dry season in Rondônia, Brazil (Hoffer et al., 2006). HULIS have been recognized as  
653 important components of BrC from biomass burning (Mukai and Ambe, 1986; Andreae and  
654 Gelencsér, 2006; Graber and Rudich, 2006). The  $E_{\text{abs}}$  value of the MO-BBOA factor was  $0.82 \pm$   
655  $0.04 \text{ m}^2 \text{ g}^{-1}$ . The result of  $E_{\text{abs,MO-BBOA}} < E_{\text{abs,LO-BBOA}}$  is consistent with an interpretation of  
656 photochemically driven oxidation and bleaching during the atmospheric transport of biomass  
657 burning emissions.

658 The  $E_{\text{abs}}$  value of the IEPOX-SOA factor was  $0.40 \pm 0.05 \text{ m}^2 \text{ g}^{-1}$ , and the  $E_{\text{abs}}$  values of  
659 the MO-OOA and LO-OOA factors ( $0.01 \pm 0.02 \text{ m}^2 \text{ g}^{-1}$ ) were not statistically different from  
660 zero. Laboratory studies suggest that biogenic PM does not appreciably absorb light in the near-  
661 UV and visible range although this result may change with atmospheric exposure to ammonia  
662 and amines, changes in particle acidity, and other factors (Nakayama et al., 2012; Liu et al.,  
663 2013; Flores et al., 2014; Lin et al., 2014; Laskin et al., 2015). Biogenic PM is typically  
664 characterized by carbonyls, carboxyls, and hydroxyls without substantial conjugation; this  
665 composition does not have the low-energy electronic transitions relevant for brown-carbon light  
666 absorption (Laskin et al., 2015). By contrast, PM produced by the photo-oxidation of aromatic  
667 VOCs, such as toluene, *m*-xylene, naphthalene, and trimethylbenzene, tends to absorb



668 significantly, and the light absorption is greater for PM produced under conditions of higher  $\text{NO}_x$   
669 concentrations because of the production of nitro-aromatic compounds (Zhong and Jang, 2011;  
670 Liu et al., 2012; Lee et al., 2014; Liu et al., 2015). This absorption, however, may decrease with  
671 atmospheric processing as previously discussed for the case of biomass burning emissions,  
672 which is also reflected in the negligible value of  $E_{\text{abs}}$  for MO-OOA. In central Amazonia, the  
673 organic PM is dominated by biogenic forest precursors even in the pollution plume of Manaus,  
674 which helps to explain the negligible  $E_{\text{abs}}$  value for LO-OOA. It may also be that some aromatic  
675 PM is associated with the HOA factor, which has a high  $E_{\text{abs}}$  value.

676 A comparison of the relative contributions of PMF factor loadings to organic  $\text{PM}_{10}$  mass  
677 concentration and to light absorption is presented in Figure 15 (left and right panels,  
678 respectively). The contribution of each class of organic compounds to total absorption by organic  
679  $\text{PM}_{10}$  was estimated for each point in time by multiplication of the  $E_{\text{abs}}$  value and the loading of  
680 each PMF factor during IOP2. The means and standard deviations of the resulting percentage  
681 contributions are listed in Table 4. Biomass burning and urban emissions, as represented by the  
682 BBOA and HOA factors, appeared to contribute 80% of  $b_{\text{abs,BrC}}$  while accounting for at least  
683 30% of the organic  $\text{PM}_{10}$  mass concentration. The IEPOX-SOA factor was associated with the  
684 balance of  $b_{\text{abs,BrC}}$  while representing 16% of the organic  $\text{PM}_{10}$  mass concentration. Studies with  
685 further information on black carbon size distribution, particle mixing state, and the effect of RH  
686 on particle absorption are warranted to refine the estimates of  $E_{\text{abs}}$  for the components of organic  
687  $\text{PM}_{10}$  and therefore their contributions to BrC light absorption. A similar attribution analysis as  
688 the right panel of Figure 15 was carried out for the baseline, event, and urban clusters separately  
689 and is discussed in the Supplementary Material (Figure S15).





#### 690 4. Summary and Conclusions

691 The influence of urban and biomass burning emissions on the otherwise natural  
692 concentrations, composition, and optical properties of organic PM<sub>1</sub> in central Amazonia were  
693 investigated during the dry season. Positive-matrix factorization was used to classify the organic  
694 PM into subcomponents. The MO-OOA, LO-OOA, and IEPOX-SOA together accounted for  
695 about 62% of the organic PM. The MO-BBOA and LO-BBOA factors together accounted for  
696 31%, and HOA for the remaining 7%. An important conclusion is that the 8.5-fold increase in  
697 organic PM<sub>1</sub> concentrations between the wet and dry seasons is not all due to biomass burning,  
698 but also to a concurrent increase of biogenic secondary organic PM<sub>1</sub> of eight-fold and smaller  
699 increases in urban PM<sub>1</sub>. Reasons that possibly played a role in such increases for the dry season  
700 are: increased BVOC emissions, increased formation potential of biogenic secondary organic  
701 PM<sub>1</sub>, reduced wet and dry deposition and PBL ventilation of PM<sub>1</sub> particles, and increased  
702 partitioning due to larger organic PM<sub>1</sub> mass concentrations in the dry season.

703 The FCM clustering analysis identified the baseline, event, and urban clusters. Relative to  
704 the baseline cluster (9.2 μg m<sup>-3</sup>), both the event and the urban cluster had an increase of 3 μg m<sup>-3</sup>.  
705 For the event cluster, the increased sulfate concentrations together with only moderate increases  
706 in NO<sub>y</sub>, resulted in remarkable increases of almost 1 μg m<sup>-3</sup> (65%) in IEPOX-SOA factor  
707 loadings relative to the baseline cluster. Regarding the urban cluster, increases in the factor  
708 loadings of MO-BBOA (40 to 90%) and LO-OOA (20 to 25%) were observed in comparison to  
709 the other two clusters. At the same time, the IEPOX-SOA contribution was either the same or  
710 lower (by 40%) in absolute loadings, and always lower in relative contribution to organic PM  
711 (15% of organic PM compared to 20-30% for the other clusters). These changes in the make-up  
712 of organic PM were consistent with the changes observed for the wet season (de Sá et al., 2017;



713 de Sá et al., 2018). They were attributed partly to (i) a shift in oxidation pathways from HO<sub>2</sub>- to  
714 NO-dominant, and partly to (ii) an accelerated oxidation cycle that increases the mass  
715 concentration of secondary organic PM.

716 Optical properties of the PM<sub>1</sub> were investigated, focusing on the organic component. The  
717 BrC absorption coefficient  $b_{\text{abs,BrC}}$  had an inverse relationship with O:C ratio and a positive  
718 relationship with the C<sub>x</sub>H<sub>y</sub>O<sub>z</sub>N<sub>p</sub><sup>+</sup> family, indicating that BrC light in this region was associated  
719 with less-oxidized and N-containing organic compounds. The LO-BBOA and HOA factors had  
720 the lowest O:C ratios and highest relative contribution of C<sub>x</sub>H<sub>y</sub>O<sub>z</sub>N<sub>p</sub><sup>+</sup> family ions, suggesting that  
721 these factors represent BrC components. In addition, a tight relationship between  $\hat{a}_{\text{abs}}$  and  
722  $\log_{10}(f_{60}/f_{44})$  was found, corroborating the importance of BBOA factors for absorption properties  
723 of organic PM, and possibly providing a parameterization for  $\hat{a}_{\text{abs}}$  in the region. Further analysis  
724 determined the  $E_{\text{abs}}$  associated with each of the PMF factors. The results implied that the MO-  
725 OOA and LO-OOA factors were associated with non-absorbing components. The MO-BBOA  
726 ( $E_{\text{abs}} = 0.8 \text{ m}^2 \text{ g}^{-1}$ ), LO-BBOA ( $1.5 \text{ m}^2 \text{ g}^{-1}$ ), and HOA ( $2.0 \text{ m}^2 \text{ g}^{-1}$ ) factors were associated with  
727 80% of the light absorption by organic PM in the region. The remaining absorption (<10%) was  
728 attributed to IEPOX-SOA ( $E_{\text{abs}} = 0.4 \text{ m}^2 \text{ g}^{-1}$ ).

729 The BrC light absorption can have direct and indirect effects on radiative forcing, which  
730 ought to be further investigated for the Amazon region. The inclusion of BrC absorption in  
731 models may result in a positive direct radiative forcing in regions of high BrC concentrations, in  
732 contrast to models that assume organic PM as a purely scattering component (Ramanathan and  
733 Carmichael, 2008; Myhre et al., 2013). Recent models have estimated the global BrC  
734 contribution to DRF to be in the range of 0.1 to 0.25 W m<sup>-2</sup>, corresponding to 10 to 25% of the  
735 DRF by BC (Feng et al., 2013). In addition, BrC in cloud water can absorb light and thereby



736 facilitate water evaporation and cloud dispersion (Hansen et al., 1997). This effect may  
737 compensate the cooling that aerosol particles offer by serving as seeds for cloud droplet  
738 formation and may also provide a positive feedback as increased fire activity may provoke more  
739 fire-prone conditions by suppressing precipitation (Nepstad et al., 1999; Bevan et al., 2009;  
740 Gonçalves et al., 2015; Laskin et al., 2015). Another implication is that light absorption by BrC  
741 in the ultraviolet may significantly decrease photolysis rates, thereby affecting the concentrations  
742 of precursors and oxidants such as ozone and OH radicals in the atmosphere (Li et al., 2011;  
743 Jiang et al., 2012; Laskin et al., 2015).

744         Given the importance of biomass burning and the increasing importance of urban  
745 pollution in the Amazon forest, light absorption by atmospheric particulate matter could become  
746 more prevalent in this region in the future. Further field, laboratory, and modeling studies are  
747 warranted to (i) more finely map the importance of both urban and biomass burning emissions at  
748 different locations in the Amazon region, (ii) characterize BrC components at the molecular level  
749 for structure-absorption relationships, and (iii) quantify the effects of BrC absorption on radiative  
750 forcing in the regional and global scales for current and future scenarios of increased human  
751 impacts.



### **Data availability**

The data sets used in this publication are available at the ARM Climate Research Facility database for the GoAmazon2014/5 experiment (<https://www.arm.gov/research/campaigns/amf2014goamazon>, last access: 1 August 2018).

### **Author contributions**

SSdS, LVR, and STM defined the scientific questions and scope of this study. STM, JLJ, MLA, AHG, and PA designed, planned, and supervised the broader GoAmazon2014/5 field experiment. SSdS, BBP, PCJ, and DAD carried out the AMS measurements and data processing. AS collected and quality-checked the aethalometer data. LVR performed the BrC calculations based on the aethalometer data. LDY, RW, GYV, JB, SC, YJL, SS, and HMJB performed auxiliary data collection/processing and simulations. SSdS carried out the scientific analysis involving PMF and FCM. SSdS prepared the paper with contributions from all co-authors.



## Acknowledgments

Institutional support was provided by the Central Office of the Large Scale Biosphere Atmosphere Experiment in Amazonia (LBA), the National Institute of Amazonian Research (INPA), and Amazonas State University (UEA). We acknowledge support from the Atmospheric Radiation Measurement (ARM) Climate Research Facility, a user facility of the United States Department of Energy (DOE, DE-SC0006680), Office of Science, sponsored by the Office of Biological and Environmental Research, and support from the Atmospheric System Research (ASR, DE-SC0011115, DE-SC0011105) program of that office. Additional funding was provided by the Amazonas State Research Foundation (FAPEAM 062.00568/2014 and 134/2016), the São Paulo State Research Foundation (FAPESP 2013/05014-0, 2017/17047-0 and 2013/50510-5), the USA National Science Foundation (1106400 and 1332998), and the Brazilian Scientific Mobility Program (CsF/CAPES). S. S. de Sá acknowledges support by the Faculty for the Future Fellowship of the Schlumberger Foundation. B. B. Palm acknowledges a US EPA STAR graduate fellowship (FP-91761701-0). This manuscript has not been reviewed by EPA and no endorsement should be inferred. BBP, PCJ, DAD, and JLJ were supported by DOE (BER/ASR) DE-SC0016559 and NSF AGS-1822664. Data access from the Sistema de Proteção da Amazônia (SIPAM) is gratefully acknowledged. The research was conducted under scientific license 001030/2012-4 of the Brazilian National Council for Scientific and Technological Development (CNPq).



## References

- Alves, E. G., Jardine, K., Tota, J., Jardine, A., Yáñez-Serrano, A. M., Karl, T., Tavares, J., Nelson, B., Gu, D., Stavrakou, T., Martin, S., Artaxo, P., Manzi, A., and Guenther, A.: Seasonality of isoprenoid emissions from a primary rainforest in central Amazonia, *Atmos. Chem. Phys.*, 16, 6, 3903-3925, <https://doi.org/10.5194/acp-16-3903-2016>, 2016.
- Ammerlaan, B. A. J., Holzinger, R., Jedynska, A. D., and Henzing, J. S.: Aerosol light absorption measurements with a carbon analyser—Calibration and precision estimates, *Atmos. Environ.*, 164, 1-7, <https://doi.org/10.1016/j.atmosenv.2017.05.031>, 2017.
- Andreae, M. O., Berresheim, H., Bingemer, H., Jacob, D. J., Lewis, B. L., Li, S. M., and Talbot, R. W.: The atmospheric sulfur cycle over the Amazon Basin: 2. Wet season, *J. Geophys. Res. Atmos.*, 95, D10, 16813-16824, <https://doi.org/10.1029/JD095iD10p16813> 1990.
- Andreae, M. O. and Merlet, P.: Emission of trace gases and aerosols from biomass burning, *Global biogeochem. cy.*, 15, 4, 955-966, <https://doi.org/10.1029/2000GB001382> 2001.
- Andreae, M. O., Artaxo, P., Brandão, C., Carswell, F. E., Ciccioli, P., da Costa, A. L., Culf, A. D., Esteves, J. L., Gash, J. H. C., Grace, J., Kabat, P., Lelieveld, J., Malhi, Y., Manzi, A. O., Meixner, F. X., Nobre, A. D., Nobre, C., Ruivo, M. d. L. P., Silva-Dias, M. A., Stefani, P., Valentini, R., von Jouanne, J., and Waterloo, M. J.: Biogeochemical cycling of carbon, water, energy, trace gases, and aerosols in Amazonia: The LBA-EUSTACH experiments, *J. Geophys. Res. Atmos.*, 107, D20, LBA 33-31-LBA 33-25, <https://doi.org/10.1029/2001JD000524>, 2002.
- Andreae, M. O., Rosenfeld, D., Artaxo, P., Costa, A. A., Frank, G. P., Longo, K. M., and Silva-Dias, M. A. F.: Smoking rain clouds over the Amazon, *Science*, 303, 5662, 1337-1342, <https://doi.org/10.1126/science.1092779>, 2004.
- Andreae, M. O. and Gelencsér, A.: Black carbon or brown carbon? The nature of light-absorbing carbonaceous aerosols, *Atmos. Chem. Phys.*, 6, 10, 3131-3148, <https://doi.org/10.5194/acp-6-3131-2006>, 2006.
- Andreae, M. O., Acevedo, O. C., Araújo, A., Artaxo, P., Barbosa, C. G. G., Barbosa, H. M. J., Brito, J., Carbone, S., Chi, X., Cintra, B. B. L., da Silva, N. F., Dias, N. L., Dias-Júnior, C. Q., Ditas, F., Ditz, R., Godoi, A. F. L., Godoi, R. H. M., Heimann, M., Hoffmann, T., Kesselmeier, J., Könemann, T., Krüger, M. L., Lavric, J. V., Manzi, A. O., Lopes, A. P., Martins, D. L., Mikhailov, E. F., Moran-Zuloaga, D., Nelson, B. W., Nölscher, A. C., Santos Nogueira, D., Piedade, M. T. F., Pöhlker, C., Pöschl, U., Quesada, C. A., Rizzo, L. V., Ro, C. U., Ruckteschler, N., Sá, L. D. A., de Oliveira Sá, M., Sales, C. B., dos Santos, R. M. N., Saturno, J., Schöngart, J., Sörgel, M., de Souza, C. M., de Souza, R. A. F., Su, H., Targhetta, N., Tóta, J., Trebs, I., Trumbore, S., van Eijck, A., Walter, D., Wang, Z., Weber, B., Williams, J., Winderlich, J., Wittmann, F., Wolff, S., and Yáñez-Serrano, A. M.: The Amazon Tall Tower Observatory (ATTO): overview of pilot measurements on ecosystem ecology, meteorology, trace gases, and aerosols, *Atmos. Chem. Phys.*, 15, 18, 10723-10776, <https://doi.org/10.5194/acp-15-10723-2015>, 2015.



- Aragão, L. E. O. C., Poulter, B., Barlow, J. B., Anderson, L. O., Malhi, Y., Saatchi, S., Phillips, O. L., and Gloor, E.: Environmental change and the carbon balance of Amazonian forests, *Biol. Rev.*, 89, 4, 913-931, <https://doi.org/10.1111/brv.12088>, 2014.
- Artaxo, P., Gerab, F., Yamasoe, M. A., and Martins, J. V.: Fine mode aerosol composition at three long-term atmospheric monitoring sites in the Amazon Basin, *J. Geophys. Res. Atmos.*, 99, D11, 22857-22868, <https://doi.org/10.1029/94JD01023> 1994.
- Artaxo, P., Martins, J. V., Yamasoe, M. A., Procópio, A. S., Pauliquevis, T. M., Andreae, M. O., Guyon, P., Gatti, L. V., and Leal, A. M. C.: Physical and chemical properties of aerosols in the wet and dry seasons in Rondônia, Amazonia, *J. Geophys. Res. Atmos.*, 107, D20, LBA 49-41-LBA 49-14, <https://doi.org/10.1029/2001JD000666>, 2002.
- Artaxo, P., Rizzo, L. V., Brito, J. F., Barbosa, H. M. J., Arana, A., Sena, E. T., Cirino, G. G., Bastos, W., Martin, S. T., and Andreae, M. O.: Atmospheric aerosols in Amazonia and land use change: from natural biogenic to biomass burning conditions, *Faraday Disc.*, 165, 0, 203-235, <https://doi.org/10.1039/C3FD00052D>, 2013.
- Bahadur, R., Praveen, P. S., Xu, Y., and Ramanathan, V.: Solar absorption by elemental and brown carbon determined from spectral observations, *Proc. Natl. Acad. Sci. USA*, 109, 43, 17366-17371, <https://doi.org/10.1073/pnas.1205910109>, 2012.
- Bevan, S., L., North, P. R. J., Grey, W. M. F., Los Sietse, O., and Plummer, S. E.: Impact of atmospheric aerosol from biomass burning on Amazon dry-season drought, *J. Geophys. Res. Atmos.*, 114, D9, D09204, <https://doi.org/10.1029/2008JD011112>, 2009.
- Bond, T. C., Zarzycki, C., Flanner, M. G., and Koch, D. M.: Quantifying immediate radiative forcing by black carbon and organic matter with the Specific Forcing Pulse, *Atmos. Chem. Phys.*, 11, 4, 1505-1525, <https://doi.org/10.5194/acp-11-1505-2011>, 2011.
- Brito, J., Rizzo, L. V., Morgan, W. T., Coe, H., Johnson, B., Haywood, J., Longo, K., Freitas, S., Andreae, M. O., and Artaxo, P.: Ground-based aerosol characterization during the South American Biomass Burning Analysis (SAMBBA) field experiment, *Atmos. Chem. Phys.*, 14, 22, 12069-12083, <https://doi.org/10.5194/acp-14-12069-2014>, 2014.
- Canagaratna, M. R., Jimenez, J. L., Kroll, J. H., Chen, Q., Kessler, S. H., Massoli, P., Hildebrandt Ruiz, L., Fortner, E., Williams, L. R., Wilson, K. R., Surratt, J. D., Donahue, N. M., Jayne, J. T., and Worsnop, D. R.: Elemental ratio measurements of organic compounds using aerosol mass spectrometry: characterization, improved calibration, and implications, *Atmos. Chem. Phys.*, 15, 1, 253-272, <https://doi.org/10.5194/acp-15-253-2015>, 2015.
- Chakrabarty, R. K., Moosmüller, H., Chen, L.-W. A., Lewis, K., Arnott, W. P., Mazzoleni, C., Dubey, M. K., Wold, C. E., Hao, W. M., and Kreidenweis, S. M.: Brown carbon in tar balls from smoldering biomass combustion, *Atmos. Chem. Phys.*, 10, 13, 6363-6370, <https://doi.org/10.5194/acp-10-6363-2010>, 2010.



- Chakraborty, S., Schiro, K. A., Fu, R., and Neelin, J. D.: On the role of aerosols, humidity, and vertical wind shear in the transition of shallow-to-deep convection at the Green Ocean Amazon 2014/5 site, *Atmos. Chem. Phys.*, 18, 15, 11135-11148, <https://doi.org/10.5194/acp-18-11135-2018>, 2018.
- Chen, Q., Farmer, D. K., Schneider, J., Zorn, S. R., Heald, C. L., Karl, T. G., Guenther, A., Allan, J. D., Robinson, N., Coe, H., Kimmel, J. R., Pauliquevis, T., Borrmann, S., Pöschl, U., Andreae, M. O., Artaxo, P., Jimenez, J. L., and Martin, S. T.: Mass spectral characterization of submicron biogenic organic particles in the Amazon Basin, *Geophys. Res. Lett.*, 36, 20, L20806, <https://doi.org/10.1029/2009GL039880>, 2009.
- Cirino, G. G., Brito, J., Barbosa, H. M. J., Rizzo, L. V., Tunved, P., de Sá, S. S., Jimenez, J. L., Palm, B. B., Carbone, S., Lavric, J., Souza, R. A. F., Wolff, S., Walter, D., Tota, J., Oliveira, M. B. L., Martin, S. T., and Artaxo, P.: Observations of Manaus urban plume evolution and interaction with biogenic emissions in GoAmazon 2014/5, *Atmos. Environ.*, <https://doi.org/10.1016/j.atmosenv.2018.08.031>, 2018.
- Claeys, M., Vermeylen, R., Yasmeen, F., Gómez-González, Y., Chi, X., Maenhaut, W., Mészáros, T., and Salma, I.: Chemical characterisation of humic-like substances from urban, rural and tropical biomass burning environments using liquid chromatography with UV/vis photodiode array detection and electrospray ionisation mass spectrometry, *Environ. Chem.*, 9, 3, 273-284, <https://doi.org/10.1071/EN11163>, 2012.
- Collaud Coen, M., Weingartner, E., Apituley, A., Ceburnis, D., Fierz-Schmidhauser, R., Flentje, H., Henzing, J. S., Jennings, S. G., Moerman, M., Petzold, A., Schmid, O., and Baltensperger, U.: Minimizing light absorption measurement artifacts of the Aethalometer: evaluation of five correction algorithms, *Atmos. Meas. Techn.*, 3, 2, 457-474, <https://doi.org/10.5194/amt-3-457-2010>, 2010.
- Collier, S., Zhou, S., Onasch, T. B., Jaffe, D. A., Kleinman, L., Sedlacek, A. J., Briggs, N. L., Hee, J., Fortner, E., Shilling, J. E., Worsnop, D., Yokelson, R. J., Parworth, C., Ge, X., Xu, J., Butterfield, Z., Chand, D., Dubey, M. K., Pekour, M. S., Springston, S., and Zhang, Q.: Regional influence of aerosol emissions from wildfires driven by combustion efficiency: insights from the BBOP campaign, *Environ. Sci. Technol.*, 50, 16, 8613-8622, <https://doi.org/10.1021/acs.est.6b01617>, 2016.
- Crutzen, P. J. and Andreae, M. O.: Biomass burning in the tropics: impact on atmospheric chemistry and biogeochemical cycles, *Science*, 250, 4988, 1669-1678, <https://doi.org/10.1126/science.250.4988.1669>, 1990.
- Cubison, M. J., Ortega, A. M., Hayes, P. L., Farmer, D. K., Day, D., Lechner, M. J., Brune, W. H., Apel, E., Diskin, G. S., Fisher, J. A., Fuelberg, H. E., Hecobian, A., Knapp, D. J., Mikoviny, T., Riemer, D., Sachse, G. W., Sessions, W., Weber, R. J., Weinheimer, A. J., Wisthaler, A., and Jimenez, J. L.: Effects of aging on organic aerosol from open biomass burning smoke in aircraft and laboratory studies, *Atmos. Chem. Phys.*, 11, 23, 12049-12064, <https://doi.org/10.5194/acp-11-12049-2011>, 2011.





- Davidson, E. A., de Araújo, A. C., Artaxo, P., Balch, J. K., Brown, I. F., Bustamante, M. M. C., Coe, M. T., DeFries, R. S., Keller, M., and Longo, M.: The Amazon basin in transition, *Nature*, 481, 7381, 321-328, <https://doi.org/10.1038/nature10717>, 2012.
- De Haan, D. O., Corrigan, A. L., Tolbert, M. A., Jimenez, J. L., Wood, S. E., and Turley, J. J.: Secondary organic aerosol formation by self-reactions of methylglyoxal and glyoxal in evaporating droplets, *Environ. Sci. Technol.*, 43, 21, 8184-8190, <https://doi.org/10.1021/es902152t>, 2009.
- de Sá, S. S., Palm, B. B., Campuzano-Jost, P., Day, D. A., Newburn, M. K., Hu, W., Isaacman-VanWertz, G., Yee, L. D., Thalman, R., Brito, J., Carbone, S., Artaxo, P., Goldstein, A. H., Manzi, A. O., Souza, R. A. F., Mei, F., Shilling, J. E., Springston, S. R., Wang, J., Surratt, J. D., Alexander, M. L., Jimenez, J. L., and Martin, S. T.: Influence of urban pollution on the production of organic particulate matter from isoprene epoxydiols in central Amazonia, *Atmos. Chem. Phys.*, 17, 11, 6611-6629, <https://doi.org/10.5194/acp-17-6611-2017>, 2017.
- de Sá, S. S., Palm, B. B., Campuzano-Jost, P., Day, D. A., Hu, W., Isaacman-VanWertz, G., Yee, L. D., Brito, J., Carbone, S., Ribeiro, I. O., Cirino, G. G., Liu, Y. J., Thalman, R., Sedlacek, A., Funk, A., Schumacher, C., Shilling, J. E., Schneider, J., Artaxo, P., Goldstein, A. H., Souza, R. A. F., Wang, J., McKinney, K. A., Barbosa, H., Alexander, M. L., Jimenez, J. L., and Martin, S. T.: Urban influence on the concentration and composition of submicron particulate matter in central Amazonia, *Atmos. Chem. Phys. Discuss.*, 2018, 1-56, <https://doi.org/10.5194/acp-2018-172>, 2018.
- DeCarlo, P. F., Kimmel, J. R., Trimborn, A., Northway, M. J., Jayne, J. T., Aiken, A. C., Gonin, M., Fuhrer, K., Horvath, T., Docherty, K. S., Worsnop, D. R., and Jimenez, J. L.: Field-deployable, high-resolution, time-of-flight aerosol mass spectrometer, *Anal. Chem.*, 78, 24, 8281-8289, <https://doi.org/10.1021/ac061249n>, 2006.
- Desyaterik, Y., Sun, Y., Shen, X., Lee, T., Wang, X., Wang, T., and Collett, J. L.: Speciation of “brown” carbon in cloud water impacted by agricultural biomass burning in eastern China, *J. Geophys. Res. Atmos.*, 118, 13, 7389-7399, <https://doi.org/10.1002/jgrd.50561>, 2013.
- Draxler, R. and Hess, G.: An overview of the HYSPLIT\_4 modeling system for trajectories, dispersion, and deposition, *Aust. Met. Mag.*, 47, 295-308, <https://doi.org/10.5194/acp-13-8607-2013>, 1998.
- Echalar, F., Artaxo, P., Martins, J. V., Yamasoe, M., Gerab, F., Maenhaut, W., and Holben, B.: Long-term monitoring of atmospheric aerosols in the Amazon Basin: Source identification and apportionment, *J. Geophys. Res. Atmos.*, 103, D24, 31849-31864, <https://doi.org/10.1029/98JD01749>, 1998.
- Farmer, D. K., Matsunaga, A., Docherty, K. S., Surratt, J. D., Seinfeld, J. H., Ziemann, P. J., and Jimenez, J. L.: Response of an aerosol mass spectrometer to organonitrates and organosulfates and implications for atmospheric chemistry, *Proc. Natl. Acad. Sci. USA*, 107, 15, 6670-6675, <https://doi.org/10.1073/pnas.0912340107>, 2010.



- Feng, Y., Ramanathan, V., and Kotamarthi, V. R.: Brown carbon: a significant atmospheric absorber of solar radiation?, *Atmos. Chem. Phys.*, 13, 17, 8607-8621, <https://doi.org/10.5194/acp-13-8607-2013>, 2013.
- Fiedler, V., Arnold, F., Ludmann, S., Minikin, A., Hamburger, T., Pirjola, L., Dörnbrack, A., and Schlager, H.: African biomass burning plumes over the Atlantic: aircraft based measurements and implications for H<sub>2</sub>SO<sub>4</sub> and HNO<sub>3</sub> mediated smoke particle activation, *Atmos. Chem. Phys.*, 11, 7, 3211-3225, <https://doi.org/10.5194/acp-11-3211-2011>, 2011.
- Flores, J. M., Washenfelder, R., Adler, G., Lee, H., Segev, L., Laskin, J., Laskin, A., Nizkorodov, S., Brown, S., and Rudich, Y.: Complex refractive indices in the near-ultraviolet spectral region of biogenic secondary organic aerosol aged with ammonia, *Phys. Chem. Chem. Phys.*, 16, 22, 10629-10642, <https://doi.org/10.1039/C4CP01009D>, 2014.
- Forrister, H., Liu, J., Scheuer, E., Dibb, J., Ziemba, L., Thornhill, K. L., Anderson, B., Diskin, G., Perring, A. E., Schwarz, J. P., Campuzano-Jost, P., Day, D. A., Palm, B. B., Jimenez, J. L., Nenes, A., and Weber, R. J.: Evolution of brown carbon in wildfire plumes, *Geophys. Res. Lett.*, 42, 11, 4623-4630, <https://doi.org/10.1002/2015GL063897>, 2015.
- Fry, J. L., Kiendler-Scharr, A., Rollins, A. W., Wooldridge, P. J., Brown, S. S., Fuchs, H., Dubé, W., Mensah, A., dal Maso, M., Tillmann, R., Dorn, H. P., Brauers, T., and Cohen, R. C.: Organic nitrate and secondary organic aerosol yield from NO<sub>3</sub> oxidation of β-pinene evaluated using a gas-phase kinetics/aerosol partitioning model, *Atmos. Chem. Phys.*, 9, 4, 1431-1449, <https://doi.org/10.5194/acp-9-1431-2009>, 2009.
- Fry, J. L., Draper, D. C., Zarzana, K. J., Campuzano-Jost, P., Day, D. A., Jimenez, J. L., Brown, S. S., Cohen, R. C., Kaser, L., Hansel, A., Cappellin, L., Karl, T., Hodzic Roux, A., Turnipseed, A., Cantrell, C., Lefer, B. L., and Grossberg, N.: Observations of gas- and aerosol-phase organic nitrates at BEACHON-RoMBAS 2011, *Atmos. Chem. Phys.*, 13, 17, 8585-8605, <https://doi.org/10.5194/acp-13-8585-2013>, 2013.
- Fuentes, J. D., Chamecki, M., Santos, R. M. N. d., Randow, C. V., Stoy, P. C., Katul, G., Fitzjarrald, D., Manzi, A., Gerken, T., Trowbridge, A., Freire, L. S., Ruiz-Plancarte, J., Maia, J. M. F., Tóta, J., Dias, N., Fisch, G., Schumacher, C., Acevedo, O., Mercer, J. R., and Yañez-Serrano, A. M.: Linking meteorology, turbulence, and air chemistry in the Amazon rain forest, *Bull. Am. Meteorol. Soc.*, 97, 12, 2329-2342, <https://doi.org/10.1175/bams-d-15-00152.1>, 2016.
- Fuzzi, S., Decesari, S., Facchini, M. C., Cavalli, F., Emblico, L., Mircea, M., Andreae, M. O., Trebs, I., Hoffer, A. s., Guyon, P., Artaxo, P., Rizzo, L. V., Lara, L. L., Pauliquevis, T., Maenhaut, W., Raes, N., Chi, X., Mayol-Bracero, O. L., Soto-García, L. L., Claeys, M., Kourtchev, I., Rissler, J., Swietlicki, E., Tagliavini, E., Schkolnik, G., Falkovich, A. H., Rudich, Y., Fisch, G., and Gatti, L. V.: Overview of the inorganic and organic composition of size-segregated aerosol in Rondonia, Brazil, from the biomass-burning



- period to the onset of the wet season, *J. Geophys. Res. Atmos.*, 112, D01201, <https://doi.org/10.1029/2005JD006741>, 2007.
- Gilardoni, S., Massoli, P., Paglione, M., Giulianelli, L., Carbone, C., Rinaldi, M., Decesari, S., Sandrini, S., Costabile, F., Gobbi, G. P., Pietrogrande, M. C., Visentin, M., Scotto, F., Fuzzi, S., and Facchini, M. C.: Direct observation of aqueous secondary organic aerosol from biomass-burning emissions, *Proc. Natl. Acad. Sci. USA*, 113, 36, 10013-10018, <https://doi.org/10.1073/pnas.1602212113>, 2016.
- Glasius, M., Bering, M. S., Yee, L. D., de Sá, S. S., Isaacman-VanWertz, G., Wernis, R. A., Barbosa, H. M. J., Alexander, M. L., Palm, B. B., Hu, W., Campuzano-Jost, P., Day, D. A., Jimenez, J. L., Shrivastava, M., Martin, S. T., and Goldstein, A. H.: Organosulfates in aerosols downwind of an urban region in central Amazon, *Environ. Sci. Process. Impacts*, 20, 11, 1546-1558, <https://doi.org/10.1039/C8EM00413G>, 2018.
- Gonçalves, W. A., Machado, L. A. T., and Kirstetter, P.-E.: Influence of biomass aerosol on precipitation over the Central Amazon: an observational study, *Atmos. Chem. Phys.*, 15, 12, 6789-6800, <https://doi.org/10.5194/acp-15-6789-2015>, 2015.
- Graber, E. R. and Rudich, Y.: Atmospheric HULIS: How humic-like are they? A comprehensive and critical review, *Atmos. Chem. Phys.*, 6, 3, 729-753, <https://doi.org/10.5194/acp-6-729-2006>, 2006.
- Hand, J. L. and Malm, W. C.: Review of aerosol mass scattering efficiencies from ground-based measurements since 1990, *J. Geophys. Res. Atmos.*, 112, D16, <https://doi.org/10.1029/2007JD008484>, 2007.
- Hansen, J., Sato, M., and Ruedy, R.: Radiative forcing and climate response, *J. Geophys. Res. Atmos.*, 102, D6, 6831-6864, <https://doi.org/10.1029/96JD03436>, 1997.
- Hems, R. F. and Abbatt, J. P. D.: Aqueous phase photo-oxidation of brown carbon nitrophenols: reaction kinetics, mechanism, and evolution of light absorption, *ACS Earth Space Chem.*, 2, 3, 225-234, <https://doi.org/10.1021/acsearthspacechem.7b00123>, 2018.
- Hoffer, A., Gelencsér, A., Guyon, P., Kiss, G., Schmid, O., Frank, G., Artaxo, P., and Andreae, M.: Optical properties of humic-like substances (HULIS) in biomass-burning aerosols, *Atmos. Chem. Phys.*, 6, 11, 3563-3570, <https://doi.org/10.5194/acp-6-3563-2006>, 2006.
- Holben, B. N., Setzer, A., Eck, T. F., Pereira, A., and Slutsker, I.: Effect of dry-season biomass burning on Amazon basin aerosol concentrations and optical properties, 1992–1994, *J. Geophys. Res. Atmos.*, 101, D14, 19465-19481, <https://doi.org/10.1029/96JD01114> 1996.
- Hu, W., Palm, B. B., Day, D. A., Campuzano-Jost, P., Krechmer, J. E., Peng, Z., de Sá, S. S., Martin, S. T., Alexander, M. L., Baumann, K., Hacker, L., Kiendler-Scharr, A., Koss, A. R., de Gouw, J. A., Goldstein, A. H., Seco, R., Sjostedt, S. J., Park, J. H., Guenther, A. B., Kim, S., Canonaco, F., Prévôt, A. S. H., Brune, W. H., and Jimenez, J. L.: Volatility and lifetime against OH heterogeneous reaction of ambient isoprene-epoxydiols-derived



secondary organic aerosol (IEPOX-SOA), Atmos. Chem. Phys., 16, 18, 11563-11580, <https://10.5194/acp-16-11563-2016>, 2016.

INPE: Instituto Nacional de Pesquisas Espaciais: Banco de dados de queimadas, 2018, <http://www.inpe.br/queimadas/bdqueimadas/>, last access: 1 February 2018.

IPCC: Summary for policymakers. In: Climate Change 2013 – The Physical Science Basis. Contribution of Working Group I to the Fifth Assessment Report of the Intergovernmental Panel on Climate Change [Stocker, T.F., D. Qin, G.-K. Plattner, M. Tignor, S.K. Allen, J. Boschung, A. Nauels, Y. Xia, V. Bex and P.M. Midgley (eds.)], Cambridge University Press, Cambridge, United Kingdom, and New York, NY, USA, Cambridge, 2013.

Isaacman-VanWertz, G., Yee, L. D., Kreisberg, N. M., Wernis, R., Moss, J. A., Hering, S. V., de Sá, S. S., Martin, S. T., Alexander, M. L., Palm, B. B., Hu, W., Campuzano-Jost, P., Day, D. A., Jimenez, J. L., Riva, M., Surratt, J. D., Viegas, J., Manzi, A., Edgerton, E., Baumann, K., Souza, R., Artaxo, P., and Goldstein, A. H.: Ambient gas-particle partitioning of tracers for biogenic oxidation, Environ. Sci. Technol., 9952-9962, <https://doi.org/10.1021/acs.est.6b01674>, 2016.

Jen, C. N., Hatch, L. E., Selimovic, V., Yokelson, R. J., Weber, R., Fernandez, A. E., Kreisberg, N. M., Barsanti, K. C., and Goldstein, A. H.: Speciated and total emission factors of particulate organics from burning western U.S. wildland fuels and their dependence on combustion efficiency, Atmos. Chem. Phys. Discuss., 2018, 1-22, <https://doi.org/10.5194/acp-2018-840>, 2018.

Jiang, X., Wiedinmyer, C., and Carlton, A. G.: Aerosols from fires: an examination of the effects on ozone photochemistry in the western United States, Environ. Sci. Technol., 46, 21, 11878-11886, <https://doi.org/10.1021/es301541k>, 2012.

Jimenez, J. L., Canagaratna, M. R., Donahue, N. M., Prevot, A. S. H., Zhang, Q., Kroll, J. H., DeCarlo, P. F., Allan, J. D., Coe, H., Ng, N. L., Aiken, A. C., Docherty, K. S., Ulbrich, I. M., Grieshop, A. P., Robinson, A. L., Duplissy, J., Smith, J. D., Wilson, K. R., Lanz, V. A., Hueglin, C., Sun, Y. L., Tian, J., Laaksonen, A., Raatikainen, T., Rautiainen, J., Vaattovaara, P., Ehn, M., Kulmala, M., Tomlinson, J. M., Collins, D. R., Cubison, M. J., Dunlea, J., Huffman, J. A., Onasch, T. B., Alfarra, M. R., Williams, P. I., Bower, K., Kondo, Y., Schneider, J., Drewnick, F., Borrmann, S., Weimer, S., Demerjian, K., Salcedo, D., Cottrell, L., Griffin, R., Takami, A., Miyoshi, T., Hatakeyama, S., Shimono, A., Sun, J. Y., Zhang, Y. M., Dzepina, K., Kimmel, J. R., Sueper, D., Jayne, J. T., Herndon, S. C., Trimborn, A. M., Williams, L. R., Wood, E. C., Middlebrook, A. M., Kolb, C. E., Baltensperger, U., and Worsnop, D. R.: Evolution of organic aerosols in the atmosphere, Science, 326, 5959, 1525-1529, <https://doi.org/10.1126/science.1180353>, 2009.

Kahnt, A., Behrouzi, S., Vermeylen, R., Safi Shalamzari, M., Vercauteren, J., Roekens, E., Claeys, M., and Maenhaut, W.: One-year study of nitro-organic compounds and their



- relation to wood burning in PM10 aerosol from a rural site in Belgium, *Atmos. Environ.*, 81, 561-568, <https://doi.org/10.1016/j.atmosenv.2013.09.041>, 2013.
- Kaufman, Y. J., Hobbs, P. V., Kirchhoff, V. W. J. H., Artaxo, P., Remer, L. A., Holben, B. N., King, M. D., Ward, D. E., Prins, E. M., Longo, K. M., Mattos, L. F., Nobre, C. A., Spinhirne, J. D., Ji, Q., Thompson, A. M., Gleason, J. F., Christopher, S. A., and Tsay, S. C.: Smoke, Clouds, and Radiation-Brazil (SCAR-B) experiment, *J. Geophys. Res. Atmos.*, 103, D24, 31783-31808, <https://doi.org/10.1029/98JD02281> 1998.
- Kitanovski, Z., Grgić, I., Vermeylen, R., Claeys, M., and Maenhaut, W.: Liquid chromatography tandem mass spectrometry method for characterization of monoaromatic nitro-compounds in atmospheric particulate matter, *J. Chrom. A*, 1268, 35-43, <https://doi.org/10.1016/j.chroma.2012.10.021>, 2012.
- Knote, C., Hodzic, A., and Jimenez, J. L.: The effect of dry and wet deposition of condensable vapors on secondary organic aerosols concentrations over the continental US, *Atmos. Chem. Phys.*, 15, 1, 1-18, <https://doi.org/10.5194/acp-15-1-2015>, 2015.
- Kuhn, U., Ganzeveld, L., Thielmann, A., Dindorf, T., Schebeske, G., Welling, M., Sciare, J., Roberts, G., Meixner, F. X., Kesselmeier, J., Lelieveld, J., Kolle, O., Ciccioli, P., Lloyd, J., Trentmann, J., Artaxo, P., and Andreae, M. O.: Impact of Manaus city on the Amazon green ocean atmosphere: ozone production, precursor sensitivity and aerosol load, *Atmos. Chem. Phys.*, 10, 19, 9251-9282, <https://doi.org/10.5194/acp-10-9251-2010>, 2010.
- Lack, D. A., Bahreini, R., Langridge, J. M., Gilman, J. B., and Middlebrook, A. M.: Brown carbon absorption linked to organic mass tracers in biomass burning particles, *Atmos. Chem. Phys.*, 13, 5, 2415-2422, <https://doi.org/10.5194/acp-13-2415-2013>, 2013.
- Laskin, A., Laskin, J., and Nizkorodov, S. A.: Chemistry of atmospheric brown carbon, *Chem. Rev.*, 115, 10, 4335-4382, <https://doi.org/10.1021/cr5006167>, 2015.
- Lee, A. K. Y., Zhao, R., Li, R., Liggio, J., Li, S.-M., and Abbatt, J. P. D.: Formation of light absorbing organo-nitrogen species from evaporation of droplets containing glyoxal and ammonium sulfate, *Environ. Sci. Technol.*, 47, 22, 12819-12826, <https://doi.org/10.1021/es402687w>, 2013.
- Lee, H. J., Aiona, P. K., Laskin, A., Laskin, J., and Nizkorodov, S. A.: Effect of solar radiation on the optical properties and molecular composition of laboratory proxies of atmospheric brown carbon, *Environ. Sci. Technol.*, 48, 17, 10217-10226, <https://doi.org/10.1021/es502515r>, 2014.
- Li, G., Bei, N., Tie, X., and Molina, L.: Aerosol effects on the photochemistry in Mexico City during MCMA-2006/MILAGRO campaign, *Atmos. Chem. Phys.*, 11, 11, 5169, <https://doi.org/10.5194/acp-11-5169-2011>, 2011.
- Lin, J. C., Matsui, T., Pielke, R. A., and Kummerow, C.: Effects of biomass-burning-derived aerosols on precipitation and clouds in the Amazon Basin: a satellite-based empirical



- study, *J. Geophys. Res. Atmos.*, 111, D19, D19204, <https://doi.org/10.1029/2005JD006884>, 2006.
- Lin, P., Aiona, P. K., Li, Y., Shiraiwa, M., Laskin, J., Nizkorodov, S. A., and Laskin, A.: Molecular characterization of brown carbon in biomass burning aerosol particles, *Environ. Sci. Technol.*, 50, 21, 11815-11824, <https://doi.org/10.1021/acs.est.6b03024>, 2016.
- Lin, Y.-H., Budisulistiorini, S. H., Chu, K., Siejack, R. A., Zhang, H., Riva, M., Zhang, Z., Gold, A., Kautzman, K. E., and Surratt, J. D.: Light-absorbing oligomer formation in secondary organic aerosol from reactive uptake of isoprene epoxydiols, *Environ. Sci. Technol.*, 48, 20, 12012-12021, <https://doi.org/10.1021/es503142b>, 2014.
- Liu, P., Zhang, Y., and Martin, S. T.: Complex refractive indices of thin films of secondary organic materials by spectroscopic ellipsometry from 220 to 1200 nm, *Environ. Sci. Technol.*, 47, 23, 13594-13601, <https://doi.org/10.1021/es403411e>, 2013.
- Liu, P. F., Abdelmalki, N., Hung, H.-M., Wang, Y., Brune, W. H., and Martin, S. T.: Ultraviolet and visible complex refractive indices of secondary organic material produced by photooxidation of the aromatic compounds toluene and m-xylene, *Atmos. Chem. Phys.*, 15, 3, 1435-1446, <https://doi.org/10.5194/acp-15-1435-2015>, 2015.
- Liu, S., Shilling, J. E., Song, C., Hiranuma, N., Zaveri, R. A., and Russell, L. M.: Hydrolysis of organonitrate functional groups in aerosol particles, *Aerosol Sci. Technol.*, 46, 12, 1359-1369, <https://doi.org/10.1080/02786826.2012.716175>, 2012.
- Liu, Y., Brito, J., Dorris, M. R., Rivera-Rios, J. C., Seco, R., Bates, K. H., Artaxo, P., Duvoisin, S., Keutsch, F. N., Kim, S., Goldstein, A. H., Guenther, A. B., Manzi, A. O., Souza, R. A. F., Springston, S. R., Watson, T. B., McKinney, K. A., and Martin, S. T.: Isoprene photochemistry over the Amazon rain forest, *Proc. Natl. Acad. Sci. USA*, 113, 22, 6125-6130, <https://doi.org/10.1073/pnas.1524136113>, 2016.
- Ma, L. and Thompson, J. E.: Optical properties of dispersed aerosols in the near ultraviolet (355 nm): measurement approach and initial data, *Anal. Chem.*, 84, 13, 5611-5617, <https://doi.org/10.1021/ac3005814>, 2012.
- Mace, K. A., Artaxo, P., and Duce, R. A.: Water-soluble organic nitrogen in Amazon Basin aerosols during the dry (biomass burning) and wet seasons, *J. Geophys. Res. Atmos.*, 108, D16, <https://doi.org/10.1029/2003JD003557>, 2003.
- Machado, L. A. T., Laurent, H., Dessay, N., and Miranda, I.: Seasonal and diurnal variability of convection over the Amazonia: a comparison of different vegetation types and large scale forcing, *Theor. App. Climatol.*, 78, 1-3, 61-77, <https://doi.org/10.1007/s00704-004-0044-9>, 2004.
- Machado, L. A. T., Dias, M. A. F. S., Morales, C., Fisch, G., Vila, D., Albrecht, R., Goodman, S. J., Calheiros, A. J. P., Biscaro, T., Kummerow, C., Cohen, J., Fitzjarrald, D., Nascimento, E. L., Sakamoto, M. S., Cunningham, C., Chaboureaud, J.-P., Petersen, W. A., Adams, D.





- K., Baldini, L., Angelis, C. F., Sapucci, L. F., Salio, P., Barbosa, H. M. J., Landulfo, E., Souza, R. A. F., Blakeslee, R. J., Bailey, J., Freitas, S., Lima, W. F. A., and Tokay, A.: The Chuva Project: how does convection vary across Brazil?, *Bull. Am. Meteorol. Soc.*, 95, 9, 1365-1380, <https://doi.org/10.1175/bams-d-13-00084.1>, 2014.
- Maenhaut, W., Fernández-Jiménez, M. T., and Artaxo, P.: Long-term study of atmospheric aerosols in Cuiabá, Brazil: multielemental composition, sources and source apportionment, *J. Aerosol Sci.*, 30, [https://doi.org/10.1016/S0021-8502\(99\)80141-4](https://doi.org/10.1016/S0021-8502(99)80141-4), 1999.
- Martin, S. T., Andreae, M. O., Artaxo, P., Baumgardner, D., Chen, Q., Goldstein, A. H., Guenther, A., Heald, C. L., Mayol-Bracero, O. L., McMurry, P. H., Pauliquevis, T., Pöschl, U., Prather, K. A., Roberts, G. C., Saleska, S. R., Dias, M. A. S., Spracklen, D. V., Swietlicki, E., and Trebs, I.: Sources and properties of Amazonian aerosol particles, *Rev Geophys*, 48, RG2002, <https://doi.org/10.1029/2008RG000280>, 2010a.
- Martin, S. T., Andreae, M. O., Althausen, D., Artaxo, P., Baars, H., Borrmann, S., Chen, Q., Farmer, D. K., Guenther, A., Gunthe, S. S., Jimenez, J. L., Karl, T., Longo, K., Manzi, A., Müller, T., Pauliquevis, T., Petters, M. D., Prenni, A. J., Pöschl, U., Rizzo, L. V., Schneider, J., Smith, J. N., Swietlicki, E., Tota, J., Wang, J., Wiedensohler, A., and Zorn, S. R.: An overview of the Amazonian aerosol characterization experiment 2008 (AMAZE-08), *Atmos. Chem. Phys.*, 10, 23, 11415-11438, <https://doi.org/10.5194/acp-10-11415-2010>, 2010b.
- Martin, S. T., Artaxo, P., Machado, L. A. T., Manzi, A. O., Souza, R. A. F., Schumacher, C., Wang, J., Andreae, M. O., Barbosa, H. M. J., Fan, J., Fisch, G., Goldstein, A. H., Guenther, A., Jimenez, J. L., Pöschl, U., Silva Dias, M. A., Smith, J. N., and Wendisch, M.: Introduction: observations and modeling of the green ocean Amazon (GoAmazon2014/5), *Atmos. Chem. Phys.*, 16, 8, 4785-4797, <https://doi.org/10.5194/acp-16-4785-2016>, 2016.
- Martin, S. T., Artaxo, P., Machado, L., Manzi, A. O., Souza, R. A. F., Schumacher, C., Wang, J., Biscaro, T., Brito, J., Calheiros, A., Jardine, K., Medeiros, A., Portela, B., Sá, S. S. d., Adachi, K., Aiken, A. C., Albrecht, R., Alexander, L., Andreae, M. O., Barbosa, H. M. J., Buseck, P., Chand, D., Comstock, J. M., Day, D. A., Dubey, M., Fan, J., Fast, J., Fisch, G., Fortner, E., Giangrande, S., Gilles, M., Goldstein, A. H., Guenther, A., Hubbe, J., Jensen, M., Jimenez, J. L., Keutsch, F. N., Kim, S., Kuang, C., Laskin, A., McKinney, K., Mei, F., Miller, M., Nascimento, R., Pauliquevis, T., Pekour, M., Peres, J., Petäjä, T., Pöhlker, C., Pöschl, U., Rizzo, L., Schmid, B., Shilling, J. E., Dias, M. A. S., Smith, J. N., Tomlinson, J. M., Tóta, J., and Wendisch, M.: The Green Ocean Amazon Experiment (GoAmazon2014/5) observes pollution affecting gases, aerosols, clouds, and rainfall over the rain forest, *Bull. Am. Meteorol. Soc.*, 98, 5, 981-997, <https://doi.org/10.1175/bams-d-15-00221.1>, 2017.
- Middlebrook, A. M., Bahreini, R., Jimenez, J. L., and Canagaratna, M. R.: Evaluation of composition-dependent collection efficiencies for the aerodyne aerosol mass



- spectrometer using field data, *Aerosol Sci. Technol.*, 46, 3, 258-271, <https://doi.org/10.1080/02786826.2011.620041>, 2012.
- Mohr, C., Lopez-Hilfiker, F. D., Zotter, P., Prévôt, A. S. H., Xu, L., Ng, N. L., Herndon, S. C., Williams, L. R., Franklin, J. P., Zahniser, M. S., Worsnop, D. R., Knighton, W. B., Aiken, A. C., Gorkowski, K. J., Dubey, M. K., Allan, J. D., and Thornton, J. A.: Contribution of nitrated phenols to wood burning brown carbon light absorption in Detling, United Kingdom during Winter time, *Environ. Sci. Technol.*, 47, 12, 6316-6324, <https://doi.org/10.1021/es400683v>, 2013.
- Morgan, W. T., Allan, J. D., Flynn, M., Darbyshire, E., Hodgson, A., Johnson, B. T., Haywood, J. M., Freitas, S., Longo, K., Artaxo, P., and Coe, H.: Overview of the South American biomass burning analysis (SAMBBA) field experiment, *AIP Conf. Proc.*, 1527, 1, 587-590, <https://doi.org/10.1063/1.4803339>, 2013.
- Mukai, H. and Ambe, Y.: Characterization of a humic acid-like brown substance in airborne particulate matter and tentative identification of its origin, *Atmos. Environ.*, 20, 5, 813-819, [https://doi.org/10.1016/0004-6981\(86\)90265-9](https://doi.org/10.1016/0004-6981(86)90265-9), 1986.
- Myhre, G., Samset, B. H., Schulz, M., Balkanski, Y., Bauer, S., Bernsten, T. K., Bian, H., Bellouin, N., Chin, M., Diehl, T., Easter, R. C., Feichter, J., Ghan, S. J., Hauglustaine, D., Iversen, T., Kinne, S., Kirkevåg, A., Lamarque, J.-F., Lin, G., Liu, X., Lund, M. T., Luo, G., Ma, X., van Noije, T., Penner, J. E., Rasch, P. J., Ruiz, A., Seland, Å., Skeie, R. B., Stier, P., Takemura, T., Tsigaridis, K., Wang, P., Wang, Z., Xu, L., Yu, H., Yu, F., Yoon, J.-H., Zhang, K., Zhang, H., and Zhou, C.: Radiative forcing of the direct aerosol effect from AeroCom Phase II simulations, *Atmos. Chem. Phys.*, 13, 4, 1853, <https://doi.org/10.5194/acp-13-1853-2013>, 2013.
- Nakayama, T., Kondo, Y., Moteki, N., Sahu, L. K., Kinase, T., Kita, K., and Matsumi, Y.: Size-dependent correction factors for absorption measurements using filter-based photometers: PSAP and COSMOS, *J. Aerosol Sci.*, 41, 4, 333-343, <https://doi.org/10.1016/j.jaerosci.2010.01.004>, 2010.
- Nakayama, T., Sato, K., Matsumi, Y., Imamura, T., Yamazaki, A., and Uchiyama, A.: Wavelength dependence of refractive index of secondary organic aerosols generated during the ozonolysis and photooxidation of  $\alpha$ -pinene, *SOLA*, 8, 119-123, <https://doi.org/10.2151/sola.2012-030>, 2012.
- Nepstad, D. C., Verssimo, A., Alencar, A., Nobre, C., Lima, E., Lefebvre, P., Schlesinger, P., Potter, C., Moutinho, P., Mendoza, E., Cochrane, M., and Brooks, V.: Large-scale impoverishment of Amazonian forests by logging and fire, *Nature*, 398, 505, <https://doi.org/10.1038/19066>, 1999.
- Ng, N. L., Herndon, S. C., Trimborn, A., Canagaratna, M. R., Croteau, P. L., Onasch, T. B., Sueper, D., Worsnop, D. R., Zhang, Q., Sun, Y. L., and Jayne, J. T.: An Aerosol Chemical Speciation Monitor (ACSM) for routine monitoring of the composition and mass concentrations of ambient aerosol, *Aerosol Sci Technol*, 45, 7, 780-794, <https://doi.org/10.1080/02786826.2011.560211>, 2011.





- Nguyen, T. B., B., L. P., M., U. K., L., B. D., Julia, L., Alexander, L., and A., N. S.: Formation of nitrogen- and sulfur-containing light-absorbing compounds accelerated by evaporation of water from secondary organic aerosols, *J. Geophys. Res. Atmos.*, 117, D1, D01207, <https://doi.org/10.1029/2011JD016944>, 2012.
- Nozière, B., Dziedzic, P., and Córdova, A.: Formation of secondary light-absorbing “fulvic-like” oligomers: A common process in aqueous and ionic atmospheric particles?, *Geophys. Res. Lett.*, 34, 21, L21812, <https://doi.org/10.1029/2007GL031300>, 2007.
- Nunes, A. M. P., Silva Dias, M. A. F., Anselmo, E. M., and Morales, C. A.: Severe Convection Features in the Amazon Basin: A TRMM-Based 15-Year Evaluation, *Front. Earth Sci.*, 4, 37, <https://doi.org/10.3389/feart.2016.00037>, 2016.
- Palm, B. B., de Sá, S. S., Day, D. A., Campuzano-Jost, P., Hu, W., Seco, R., Sjostedt, S. J., Park, J. H., Guenther, A. B., Kim, S., Brito, J., Wurm, F., Artaxo, P., Thalman, R., Wang, J., Yee, L. D., Wernis, R., Isaacman-VanWertz, G., Goldstein, A. H., Liu, Y., Springston, S. R., Souza, R., Newburn, M. K., Alexander, M. L., Martin, S. T., and Jimenez, J. L.: Secondary organic aerosol formation from ambient air in an oxidation flow reactor in central Amazonia, *Atmos. Chem. Phys.*, 18, 1, 467-493, <https://doi.org/10.5194/acp-18-467-2018>, 2018.
- Pöhlker, M. L., Pöhlker, C., Ditas, F., Klimach, T., Hrabec de Angelis, I., Araújo, A., Brito, J., Carbone, S., Cheng, Y., Chi, X., Ditz, R., Gunthe, S. S., Kesselmeier, J., Könemann, T., Lavrič, J. V., Martin, S. T., Mikhailov, E., Moran-Zuloaga, D., Rose, D., Saturno, J., Su, H., Thalman, R., Walter, D., Wang, J., Wolff, S., Barbosa, H. M. J., Artaxo, P., Andreae, M. O., and Pöschl, U.: Long-term observations of cloud condensation nuclei in the Amazon rain forest – Part 1: Aerosol size distribution, hygroscopicity, and new model parametrizations for CCN prediction, *Atmos. Chem. Phys.*, 16, 24, 15709-15740, <https://doi.org/10.5194/acp-16-15709-2016>, 2016.
- Pöschl, U.: Aerosol particle analysis: challenges and progress, *Anal. Bioanal. Chem.*, 375, 1, 30-32, <https://doi.org/10.1007/s00216-002-1611-5>, 2003.
- Powelson, M. H., Espelien, B. M., Hawkins, L. N., Galloway, M. M., and De Haan, D. O.: Brown carbon formation by aqueous-phase carbonyl compound reactions with amines and ammonium sulfate, *Environ. Sci. Technol.*, 48, 2, 985-993, <https://doi.org/10.1021/es4038325>, 2014.
- Ramanathan, V., Li, F., Ramana, M. V., Praveen, P. S., Kim, D., Corrigan, C. E., Nguyen, H., Stone, E. A., Schauer, J. J., Carmichael, G. R., Adhikary, B., and Yoon, S. C.: Atmospheric brown clouds: Hemispherical and regional variations in long-range transport, absorption, and radiative forcing, *J. Geophys. Res. Atmos.*, 112, D22, D22S21, <https://doi.org/10.1029/2006JD008124>, 2007.
- Ramanathan, V. and Carmichael, G.: Global and regional climate changes due to black carbon, *Nat. Geosci.*, 1, 221, <https://doi.org/10.1038/ngeo156>, 2008.



- Rizzo, L. V., Correia, A. L., Artaxo, P., Procopio, A. S., and Andreae, M. O.: Spectral dependence of aerosol light absorption over the Amazon Basin, *Atmos. Chem. Phys.*, 11, 17, 8899-8912, <https://doi.org/10.5194/acp-11-8899-2011>, 2011.
- Rizzo, L. V., Artaxo, P., Mueller, T., Wiedensohler, A., Paixao, M., Cirino, G. G., Arana, A., Swietlicki, E., Roldin, P., Fors, E. O., Wiedemann, K., Leal, L. S. M., and Kulmala, M.: Long term measurements of aerosol optical properties at a primary forest site in Amazonia, *Atmos. Chem. Phys.*, 13, 5, 2391-2413, <https://doi.org/10.5194/acp-13-2391-2013>, 2013.
- Romonosky, D. E., Laskin, A., Laskin, J., and Nizkorodov, S. A.: High-resolution mass spectrometry and molecular characterization of aqueous photochemistry products of common types of secondary organic aerosols, *J. Phys Chem. A*, 119, 11, 2594-2606, <https://doi.org/10.1021/jp509476r>, 2015.
- Rummel, U., Ammann, C., Kirkman, G. A., Moura, M. A. L., Foken, T., Andreae, M. O., and Meixner, F. X.: Seasonal variation of ozone deposition to a tropical rain forest in southwest Amazonia, *Atmos. Chem. Phys.*, 7, 20, 5415-5435, <https://doi.org/10.5194/acp-7-5415-2007>, 2007.
- Saleh, R., Robinson, E. S., Tkacik, D. S., Ahern, A. T., Liu, S., Aiken, A. C., Sullivan, R. C., Presto, A. A., Dubey, M. K., Yokelson, R. J., Donahue, N. M., and Robinson, A. L.: Brownness of organics in aerosols from biomass burning linked to their black carbon content, *Nat. Geosci.*, 7, 647, <https://doi.org/10.1038/ngeo2220>, 2014.
- Saturno, J., Pöhlker, C., Massabò, D., Brito, J., Carbone, S., Cheng, Y., Chi, X., Ditas, F., de Angelis, I. H., Morán-Zuloaga, D., Pöhlker, M., Rizzo, L. V., Walter, D., Wang, Qiaoqiao, Artaxo, P., Prati, P., and Andreae, M. O.: Comparison of different Aethalometer correction schemes and a reference multi-wavelength absorption technique for ambient aerosol data, *Atmos. Meas. Tech.*, 10, 8, 2837, <https://doi.org/10.5194/amt-10-2837-2017>, 2017.
- Saturno, J., Holanda, B. A., Pöhlker, C., Ditas, F., Wang, Q., Moran-Zuloaga, D., Brito, J., Carbone, S., Cheng, Y., Chi, X., Ditas, J., Hoffmann, T., Hrabě de Angelis, I., Könemann, T., Lavrič, J. V., Ma, N., Ming, J., Paulsen, H., Pöhlker, M. L., Rizzo, L. V., Schlag, P., Su, H., Walter, D., Wolff, S., Zhang, Y., Artaxo, P., Pöschl, U., and Andreae, M. O.: Black and brown carbon over central Amazonia: Long-term aerosol measurements at the ATTO site, *Atmos. Chem. Phys.*, 18, 17, 12817-12843, <https://doi.org/10.5194/acp-18-12817-2018>, 2018a.
- Saturno, J., Ditas, F., Penning de Vries, M., Holanda, B. A., Pöhlker, M. L., Carbone, S., Walter, D., Bobrowski, N., Brito, J., Chi, X., Gutmann, A., Angelis, I. H. d., Machado, L. A. T., Moran-Zuloaga, D., Rüdiger, J., Schneider, J., Schulz, C., Wang, Q., Wendisch, M., Artaxo, P., Wagner, T., Pöschl, U., Andreae, M. O., and Pöhlker, C.: African volcanic emissions influencing atmospheric aerosols over the Amazon rain forest, *Atmos. Chem. Phys.*, 18, 14, 10391-10405, <https://doi.org/10.5194/acp-18-10391-2018>, 2018b.



- Schmid, O., Artaxo, P., Arnott, W. P., Chand, D., Gatti, L. V., Frank, G. P., Hoffer, A., Schnaiter, M., and Andreae, M. O.: Spectral light absorption by ambient aerosols influenced by biomass burning in the Amazon Basin. I: Comparison and field calibration of absorption measurement techniques, *Atmos. Chem. Phys.*, 6, 11, 3443-3462, <https://doi.org/10.5194/acp-6-3443-2006>, 2006.
- Schneider, J., Weimer, S., Drewnick, F., Borrmann, S., Helas, G., Gwaze, P., Schmid, O., Andreae, M. O., and Kirchner, U.: Mass spectrometric analysis and aerodynamic properties of various types of combustion-related aerosol particles, *Int. J. Mass Spectrom.*, 258, 1, 37-49, <https://doi.org/10.1016/j.ijms.2006.07.008>, 2006.
- Sena, E. T., Artaxo, P., and Correia, A. L.: Spatial variability of the direct radiative forcing of biomass burning aerosols and the effects of land use change in Amazonia, *Atmos. Chem. Phys.*, 13, 3, 1261-1275, <https://doi.org/10.5194/acp-13-1261-2013>, 2013.
- Setzer, A. W. and Pereira, M. C.: Amazonia biomass burnings in 1987 and an estimate of their tropospheric emissions, *Ambio*, 20, 1, 19-22, <https://doi.org/10.2307/4313765>, 1991.
- Sumlin, B. J., Pandey, A., Walker, M. J., Pattison, R. S., Williams, B. J., and Chakrabarty, R. K.: Atmospheric Photooxidation Diminishes Light Absorption by Primary Brown Carbon Aerosol from Biomass Burning, *Environ. Sci. Technol. Lett.*, 4, 12, 540-545, <https://doi.org/10.1021/acs.estlett.7b00393>, 2017.
- Sun, H., Biedermann, L., and Bond, T. C.: Color of brown carbon: A model for ultraviolet and visible light absorption by organic carbon aerosol, *Geophys. Res. Lett.*, 34, 17, L17813, <https://doi.org/doi:10.1029/2007GL029797>, 2007.
- Thalman, R., de Sá, S. S., Palm, B. B., Barbosa, H. M. J., Pöhlker, M. L., Alexander, M. L., Brito, J., Carbone, S., Castillo, P., Day, D. A., Kuang, C., Manzi, A., Ng, N. L., Sedlacek Iii, A. J., Souza, R., Springston, S., Watson, T., Pöhlker, C., Pöschl, U., Andreae, M. O., Artaxo, P., Jimenez, J. L., Martin, S. T., and Wang, J.: CCN activity and organic hygroscopicity of aerosols downwind of an urban region in central Amazonia: seasonal and diel variations and impact of anthropogenic emissions, *Atmos. Chem. Phys.*, 17, 19, 11779-11801, <https://doi.org/10.5194/acp-17-11779-2017>, 2017.
- Ulbrich, I. M., Canagaratna, M. R., Zhang, Q., Worsnop, D. R., and Jimenez, J. L.: Interpretation of organic components from positive matrix factorization of aerosol mass spectrometric data, *Atmos. Chem. Phys.*, 9, 9, 2891-2918, <https://doi.org/10.5194/acp-9-2891-2009>, 2009.
- van Marle, M. J. E., Field, R. D., Werf, G. R., Estrada de Wagt, I. A., Houghton, R. A., Rizzo, L. V., Artaxo, P., and Tsigaridis, K.: Fire and deforestation dynamics in Amazonia (1973–2014), *Global Biogeochem. Cy.*, 31, 1, 24-38, <https://doi.org/10.1002/2016GB005445>, 2017.
- Wang, X., Heald, C. L., Sedlacek, A. J., de Sá, S. S., Martin, S. T., Alexander, M. L., Watson, T. B., Aiken, A. C., Springston, S. R., and Artaxo, P.: Deriving brown carbon from multiwavelength absorption measurements: method and application to AERONET and



- Aethalometer observations, *Atmos. Chem. Phys.*, 16, 19, 12733-12752, <https://doi.org/10.5194/acp-16-12733-2016>, 2016.
- Washenfelder, R. A., Attwood, A. R., Brock, C. A., Guo, H., Xu, L., Weber, R. J., Ng, N., Allen, H. M., Ayres, B. R., Karsten, B., Cohen, R. C., Draper, D. C., Duffey, K. C., Edgerton, E., Fry, J. L., Hu, W., Jimenez, J. L., Palm, B. B., Romer, P., and Brown, S.: Biomass burning dominates brown carbon absorption in the rural southeastern United States, *Geophys. Res. Lett.*, 42, 2, <https://doi.org/10.1002/2014GL062444>, 2015.
- Weingartner, E., Saathoff, H., Schnaiter, M., Streit, N., Bitnar, B., and Baltensperger, U.: Absorption of light by soot particles: determination of the absorption coefficient by means of aethalometers, *J. Aerosol Sci.*, 34, 10, 1445-1463, [https://doi.org/10.1016/S0021-8502\(03\)00359-8](https://doi.org/10.1016/S0021-8502(03)00359-8), 2003.
- Yáñez-Serrano, A. M., Nölscher, A. C., Williams, J., Wolff, S., Alves, E., Martins, G. A., Bourtsoukidis, E., Brito, J., Jardine, K., Artaxo, P., and Kesselmeier, J.: Diel and seasonal changes of biogenic volatile organic compounds within and above an Amazonian rainforest, *Atmos. Chem. Phys.*, 15, 6, 3359-3378, <https://doi.org/10.5194/acp-15-3359-2015>, 2015.
- Yang, M., Howell, S. G., Zhuang, J., and Huebert, B. J.: Attribution of aerosol light absorption to black carbon, brown carbon, and dust in China—interpretations of atmospheric measurements during EAST-AIRE, *Atmos. Chem. Phys.*, 9, 6, 2035-2050, <https://doi.org/10.5194/acp-9-2035-2009>, 2009.
- Yee, L. D., Isaacman-VanWertz, G., Wernis, R. A., Meng, M., Rivera, V., Kreisberg, N. M., Hering, S. V., Bering, M. S., Glasius, M., Upshur, M. A., Gray Bé, A., Thomson, R. J., Geiger, F. M., Offenberg, J. H., Lewandowski, M., Kourtchev, I., Kalberer, M., de Sá, S. S., Martin, S. T., Alexander, M. L., Palm, B. B., Hu, W., Campuzano-Jost, P., Day, D. A., Jimenez, J. L., Liu, Y., McKinney, K. A., Artaxo, P., Viegas, J., Manzi, A., Oliveira, M. B., de Souza, R., Machado, L. A. T., Longo, K., and Goldstein, A. H.: Observations of sesquiterpenes and their oxidation products in central Amazonia during the wet and dry seasons, *Atmos. Chem. Phys.*, 18, 14, 10433-10457, <https://doi.org/10.5194/acp-18-10433-2018>, 2018.
- Yokelson, R. J., Karl, T., Artaxo, P., Blake, D. R., Christian, T. J., Griffith, D. W., Guenther, A., and Hao, W. M.: The tropical forest and fire emissions experiment: overview and airborne fire emission factor measurements, *Atmos. Chem. Phys.*, 7, 19, 5175-5196, <https://doi.org/10.5194/acp-7-5175-2007>, 2007.
- Zhao, R., Lee, A. K. Y., Huang, L., Li, X., Yang, F., and Abbatt, J. P. D.: Photochemical processing of aqueous atmospheric brown carbon, *Atmos. Chem. Phys.*, 15, 11, 6087-6100, <https://doi.org/10.5194/acp-15-6087-2015>, 2015.
- Zhong, M. and Jang, M.: Light absorption coefficient measurement of SOA using a UV-Visible spectrometer connected with an integrating sphere, *Atmos. Environ.*, 45, 25, 4263-4271, <https://doi.org/10.1016/j.atmosenv.2011.04.082>, 2011.



Zhou, S., Collier, S., Jaffe, D. A., Briggs, N. L., Hee, J., Sedlacek III, A. J., Kleinman, L., Onasch, T. B., and Zhang, Q.: Regional influence of wildfires on aerosol chemistry in the western US and insights into atmospheric aging of biomass burning organic aerosol, Atmos. Chem. Phys., 17, 3, 2477-2493, <https://doi.org/10.5194/acp-17-2477-2017>, 2017.



## List of Tables

**Table 1.** Characteristics of the PMF factor profiles. Listed are  $f_{44}$  and  $f_{60}$ , corresponding to the organic signal fraction at  $m/z$  44 and  $m/z$  60, respectively, as well as the oxygen-to-carbon (O:C) and hydrogen-to-carbon (H:C) ratios. Values and uncertainties were calculated by running the PMF analysis in “bootstrap mode” (Ulbrich et al., 2009). The Pearson- $R$  correlations between the factor profiles of IOP2 and their counterparts in IOP1 are also listed (i.e., dry season compared to wet season). “N/A” means “not applicable”. Elemental ratios were calibrated by the “improved-ambient” method, which has an estimated uncertainty of 12% for O:C and 4% for H:C (Canagaratna et al., 2015).

PMF factor	$f_{44}$	$f_{60}$	O:C	H:C	Pearson- $R$ against IOP1 counterpart
MO-OOA	$0.24 \pm 0.01$	$< 0.001$	$1.20 \pm 0.10$	$1.25 \pm 0.08$	1.00
LO-OOA	$0.15 \pm 0.01$	$0.001 \pm 0.001$	$0.86 \pm 0.08$	$1.51 \pm 0.06$	0.99
IEPOX-SOA	$0.14 \pm 0.01$	$< 0.001$	$0.74 \pm 0.02$	$1.51 \pm 0.01$	0.99
MO-BBOA	$0.13 \pm 0.01$	$0.011 \pm 0.003$	$0.70 \pm 0.07$	$1.59 \pm 0.11$	N/A
LO-BBOA	$0.02 \pm 0.01$	$0.05 \pm 0.01$	$0.53 \pm 0.04$	$1.79 \pm 0.06$	N/A
HOA	$0.05 \pm 0.01$	$0.001 \pm 0.001$	$0.22 \pm 0.03$	$1.82 \pm 0.03$	0.94



**Table 2.** Relationship of PMF factors to organo-nitrogen characteristics. Listed for each factor are the mean loading of the time series, the percent contribution of the  $C_xH_yO_zN_p^+$  family to the factor profile, the mean mass concentration of the  $C_xH_yO_zN_p^+$  family (based on multiplication of columns 2 and 3), as well as the Pearson-*R* correlation of factor loading against the mass concentration of  $C_xH_yO_zN_p^+$ , the mass concentration of organic nitrates, and  $b_{\text{abs,BrC}}$ . The  $C_xH_yO_zN_p^+$  family corresponds to the sum of all ions containing at least one C atom and one N atom, as measured by the AMS. Detailed family-colored spectra showing the nitrogen-containing ions for all PMF factors are presented in Figure S6, and the most important ion fits are shown in Figure S7. The AMS method characterizes organic nitrates through the  $\text{NO}^+$  and  $\text{NO}_2^+$  fragments, which remain distinct from the larger fragments of the  $C_xH_yO_zN_p^+$  family (Section S1 and discussion therein).

PMF factor	Mean factor loading ( $\mu\text{g m}^{-3}$ )	Nitrogen characteristics of factor profile		Pearson <i>R</i> of factor loading		
		$C_xH_yO_zN_p^+$ family contribution (%)	Mass concentration of the $C_xH_yO_zN_p^+$ family ( $\mu\text{g m}^{-3}$ )	Against the mass concentration of $C_xH_yO_zN_p^+$ family	Against the mass concentration of organic nitrates	Against $b_{\text{abs,BrC}}$
MO-OOA	1.6	5.7	0.09	0.33	0.38	0.17
LO-OOA	2.2	3.7	0.08	0.10	0.15	-0.19
IEPOX-SOA	1.2	6.6	0.08	0.39	0.40	0.17
MO-BBOA	1.5	2.9	0.04	0.65	0.24	0.53



LO-BBOA	1.0	10.4	0.11	0.89	0.13	0.69
HOA	0.6	9.0	0.05	0.82	0.20	0.68

**Table 3.** Results of the constrained linear least squares regression analysis for the brown-carbon absorption coefficient (Equation 5). (a) Mass absorption efficiency  $E_{\text{abs}}$  associated with each PMF factor. (b) Model intercept. The mean, standard error (SE), and 95% confidence interval (CI) are listed in each panel. Unit of  $\text{Mm}^{-1}$  represents  $10^{-6} \text{ m}^{-1}$ . The coefficient of determination  $R^2$  between predicted  $b_{\text{abs,BrC,pred}}$  and observed  $b_{\text{abs,BrC}}$  was 0.66. The symbol “\*” indicates that the estimated value was statistically not higher than zero.

(a)	$E_{\text{abs}} (\text{m}^2 \text{ g}^{-1})$		
	PMF factors	Mean	SE
MO-OOA	0.01*	0.02	[0.00, 0.08]
LO-OOA	0.01*	0.02	[0.00, 0.08]
IEPOX-SOA	0.40	0.05	[0.31, 0.50]
MO-BBOA	0.82	0.04	[0.75, 0.90]
LO-BBOA	1.50	0.07	[1.37, 1.63]
HOA	2.04	0.14	[1.76, 2.31]
(b)	$b_{\text{abs}} (\text{Mm}^{-1})$		
	Model intercept	Mean	SE
$B$	0.13*	0.10	[0.00, 0.33]





**Table 4.** Contribution of PM<sub>1</sub> components as represented by the PMF factors to organic mass concentrations and BrC light absorption. The contribution of the model intercept to BrC light absorption is also included. Values listed are resulting means and standard deviations of the contributions calculated throughout IOP2. Small differences between the values in column 2 and the values represented in the inset of Figure 5a are due to differences in data coverage by the aethalometer and AMS.

PMF factor	Contribution to organic mass concentration (%)	Contribution to BrC light absorption (%)
MO-OOA	21.1 ± 10.0	0.5 ± 0.4
LO-OOA	30.9 ± 11.4	0.8 ± 0.5
IEPOX-SOA	16.3 ± 9.8	15.7 ± 11.2
MO-BBOA	16.7 ± 12.0	28.9 ± 18.0
LO-BBOA	9.5 ± 7.5	27.8 ± 14.3
HOA	5.5 ± 3.9	21.7 ± 10.5
Model intercept	N/A	4.6 ± 2.6



## List of Figures

- Figure 1.** PM<sub>1</sub> composition during the dry season from August 15 to October 15, 2014, representing the second Intensive Operating Period (IOP2) of the GoAmazon2014/5 experiment. Results are shown for measurements at T3 in comparison to other sites. (a) PM<sub>1</sub> mass concentrations of non-refractory AMS organic, sulfate, ammonium, nitrate, and chloride. Mass concentrations of SP2 refractory black carbon (rBC) are also plotted. rBC refers to the carbon content of graphite-like components that are strongly light-absorbing (Pöschl, 2003). (b) (Top) Summed mass concentrations and (bottom) segregated mass fractions of the non-refractory species at the T0a, T2, and T3 sites. The inset of panel a shows the locations of the relevant research sites for this study. A larger map is shown in Figure 3. T0a is the Amazonian Tall Tower Observatory (Andreae et al., 2015). T2 is a site 8 km downwind of Manaus, just across the Black River (“Rio Negro”) (Cirino et al., 2018). Measurements at T0a and T2 were made by an ACSM. Concentrations in both panels were adjusted to standard temperature (273.15 K) and pressure (10<sup>5</sup> Pa) (STP).
- Figure 2.** Time series of (a) organic and (b) sulfate mass concentrations at the T0a, T2, and T3 sites. Concentrations were adjusted to standard temperature (273.15 K) and pressure (10<sup>5</sup> Pa).
- Figure 3.** Fire locations in the upwind region of the T3 site for each week of IOP2. Transport times from the fires to the T3 site represent up to 15 h at the scale of this figure and typical wind speeds. The plotted data was obtained from the fire database of the Brazilian National Institute of Spatial Research (INPE, 2018). Underlying image: Google Maps.



**Figure 4.** Diel trends of (top) organic and (bottom) sulfate mass concentrations at the T0a, T2, and T3 sites. Lines represent means, solid markers show medians, and boxes span interquartile ranges. Local time is UTC minus 4 h. Concentrations were adjusted to standard temperature (273.15 K) and pressure ( $10^5$  Pa).

**Figure 5.** PMF analysis of the time series of AMS organic mass spectra collected at the T3 site. (a) Mass spectral profile of each factor represented at unit mass resolution. The inset shows the mean fractional loading of each factor. The factor profiles are shown in more detail, colored by ion families, in Figure S5. (b) Diel trends for the loadings of each PMF factor. Local time is UTC minus 4 h. Lines represent means, solid markers show medians, and boxes span interquartile ranges. (c) Time series of the factor loadings.

**Figure 6.** Pearson-*R* correlations between the loading of each PMF factor and concentrations of selected measurements at the T3 site. Abbreviations include tricarballic acid (TCA), methyl-butyl-tricarboxylic acid (MBTCA), methyl vinyl ketone (MVK), methacrolein (MACR), isoprene hydroxyhydroperoxides (ISOPOOH), and refractory black carbon (rBC). SV-TAG measurements refer to particle-phase concentrations, except for sesquiterpenes which refer to total concentrations and mostly occurred in the gas phase. The  $C_8$  and  $C_9$  aromatics include the xylene and trimethylbenzene isomers, respectively. The  $C_{20}$ ,  $C_{22}$ , and  $C_{24}$  acids include eicosanoic, docosanoic, and tetracosanoic acids, respectively.

**Figure 7.** Analysis of the organic  $PM_{10}$  sampled at the T3 site in relation to biomass burning. (a) Scatter plot of the AMS signal fraction at  $m/z$  44 ( $f_{44}$ ) against that at  $m/z$  60 ( $f_{60}$ ). Red circles represent measurements during the dry season (IOP2), and blue squares



represent measurements at the same site during the wet season (IOP1) (de Sá et al., 2018). Diamonds represent the MO-BBOA and LO-BBOA factors of IOP2. The dashed line represents a reference for negligible influence by biomass burning based on several field studies (Cubison et al., 2011). (b) Diel trends of the fractional loadings of the MO-BBOA and LO-BBOA factors relative to their sum  $BBOA_T$ . Local time is UTC minus 4 h.

**Figure 8.** Results of the cluster analysis by Fuzzy c-means (FCM) for afternoon periods (12:00 to 16:00) presented by several case studies. The shown case studies represent 30% of the FCM results. (a) Degree of membership in each of the three clusters. The sum of degrees of membership across all clusters is unity. (b) Pollution indicators: concentrations of  $NO_3$ ,  $O_3$ , CO, refractory black carbon (rBC), and particle number count are plotted. (c)  $PM_{10}$  mass concentrations for organic, sulfate, nitrate, and ammonium species. (d) Fractional contribution of each factor to the  $PM_{10}$  organic mass concentration.

**Figure 9.** Air-mass backtrajectories associated with the three clusters of the FCM analysis. Trajectories were calculated using HYSPLIT4 in steps of 12 min for 10 h (Draxler and Hess, 1998). Twenty trajectories are plotted for each cluster, corresponding to the times of highest degree of membership to that cluster.

**Figure 10.**  $PM_{10}$  characterization represented by the centroids of the FCM clusters. (a) Mass concentrations of AMS species. (b) PMF factor loadings. Results are for afternoon time periods. Table S1 lists the values presented in this figure.

**Figure 11.** Diel trends of  $PM_{10}$  optical properties. (a) Total absorption coefficient  $b_{abs}$  (370 nm). (b) Absorption coefficient  $b_{abs,BrC}$  of brown carbon (370 nm). (c) Fractional



contribution of  $b_{\text{abs,BrC}}$  to  $b_{\text{abs}}$ . (d) Absorption Ångstrom exponent  $\hat{a}_{\text{abs}}$  from 370 to 430 nm. Local time is UTC minus 4 h.

**Figure 12.** Relationships between the brown-carbon absorption coefficient and the organic PM<sub>1</sub> composition. Scatter plots of  $b_{\text{abs,BrC}}$  against (a) the oxygen-to-carbon ratio (O:C) and (b) the mass concentration of the nitrogen-containing  $\text{C}_x\text{H}_y\text{O}_z\text{N}_p^+$  family. For the  $\text{C}_x\text{H}_y\text{O}_z\text{N}_p^+$  family, all ions contain at least one C atom and one N atom, meaning  $x > 0$ ,  $y \geq 0$ ,  $z \geq 0$ , and  $p > 0$ . Boxes indicate interquartile ranges, and horizontal lines within the boxes indicate medians. In complement, Figure S14 shows the relationships between the brown-carbon absorption coefficient and the fractional contributions of the  $\text{C}_x\text{H}_y\text{O}_z^+$  and  $\text{C}_x\text{H}_y\text{O}_z\text{N}_p^+$  families to organic PM<sub>1</sub>.

**Figure 13.** Relationships between the absorption Ångstrom exponent and indicators of biomass burning. Scatter plots of  $\hat{a}_{\text{abs}}$  against (a)  $\log_{10}(f_{60}/f_{44})$  of the AMS analysis ( $R = 0.87$ ), and (b) the ratio of the BBOA<sub>T</sub> loading to the organic PM<sub>1</sub> mass concentration ( $R = 0.75$ ). BBOA<sub>T</sub> loading is the sum of the MO-BBOA and LO-BBOA factor loadings. The  $\hat{a}_{\text{abs}}$  value corresponds to 370 to 430 nm. In panel a, the slope and intercept are  $3.2 \pm 0.1$  and  $6.8 \pm 0.1$ , respectively. In panel b, they are  $5.2 \pm 0.1$  and  $1.1 \pm 0.1$ .

**Figure 14.** Scatter plots against  $b_{\text{abs,BrC}}$  of (a-f) PMF factor loadings, (g) organic PM<sub>1</sub> mass concentration, and (h)  $b_{\text{abs,BrC,pred}}$  values predicted by a multivariate linear regression model using PMF factor loadings as parameters as described by Equation 5.

**Figure 15.** Comparative relationship of the relative contributions of PMF factor loadings to (left) organic PM<sub>1</sub> mass concentration and (right) organic PM<sub>1</sub> light absorption. Results represent means for the full datasets of IOP2. The means and standard



deviations are listed in Table 4. Results are for 370 nm. “Other” refers to the model intercept  $B$  (Equation 5).

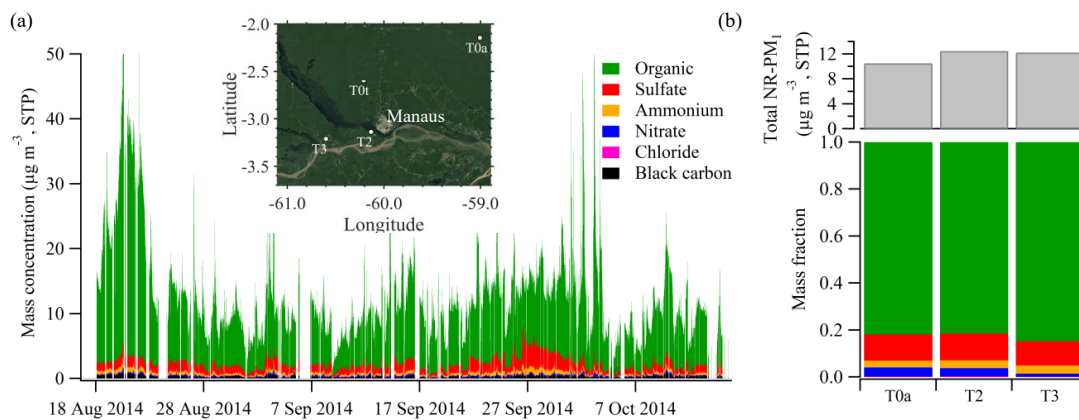


Figure 1

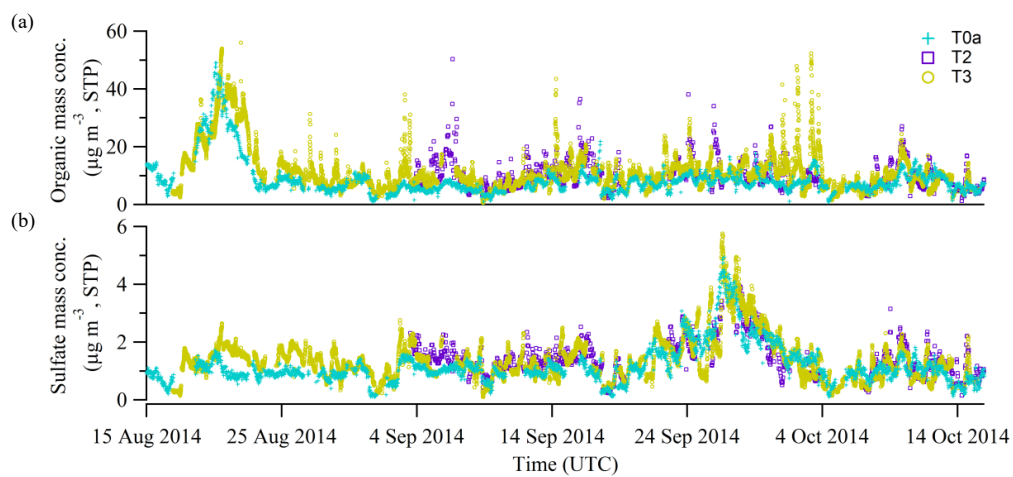


Figure 2



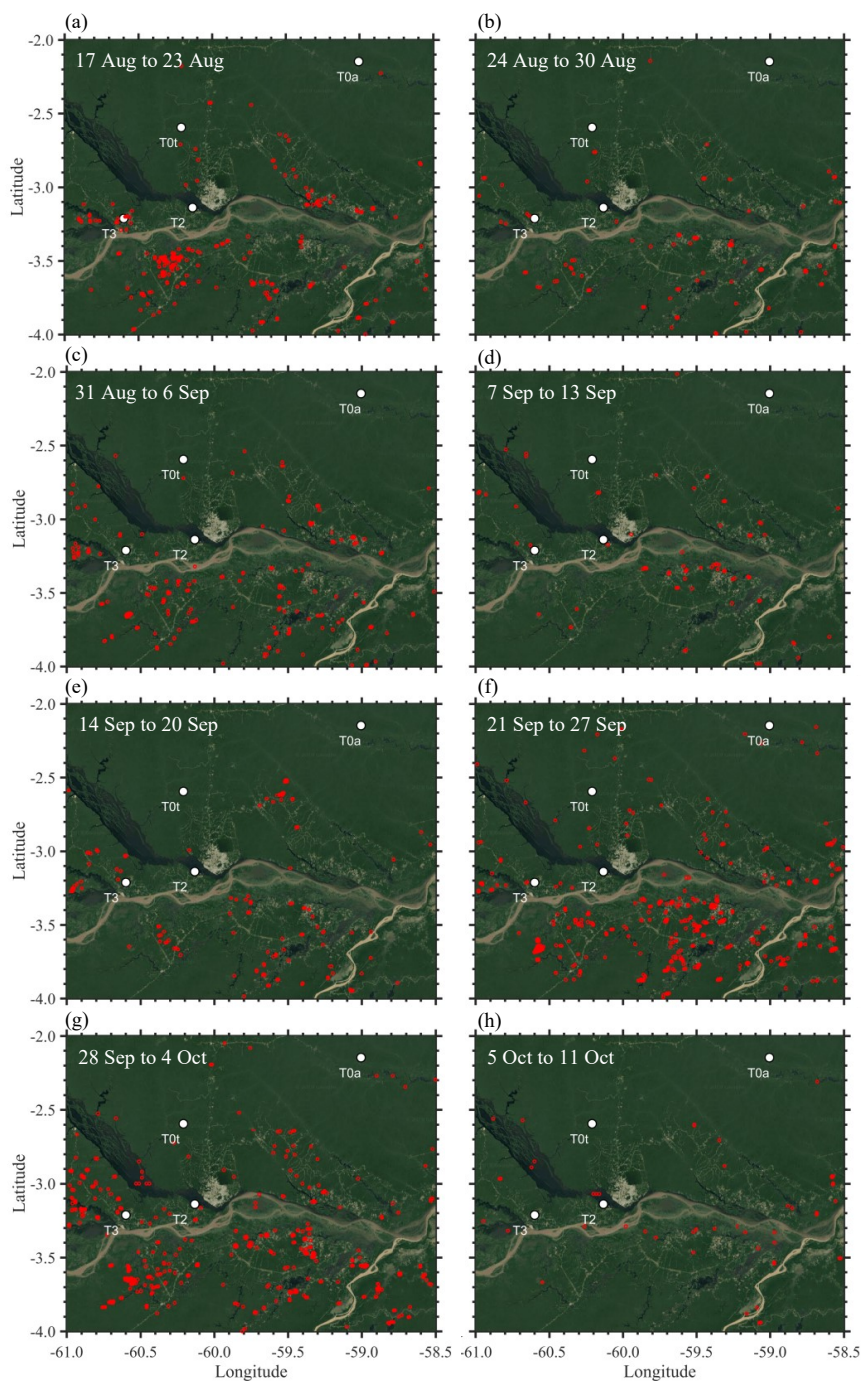


Figure 3

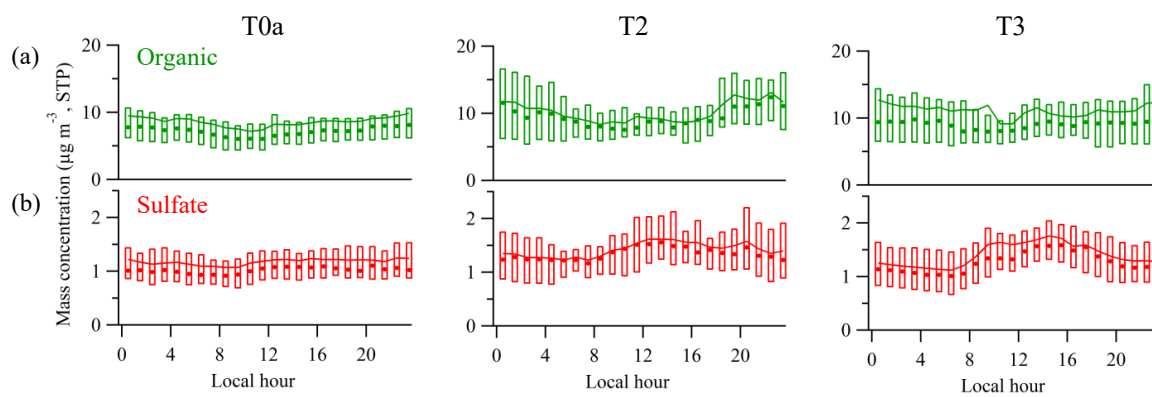


Figure 4

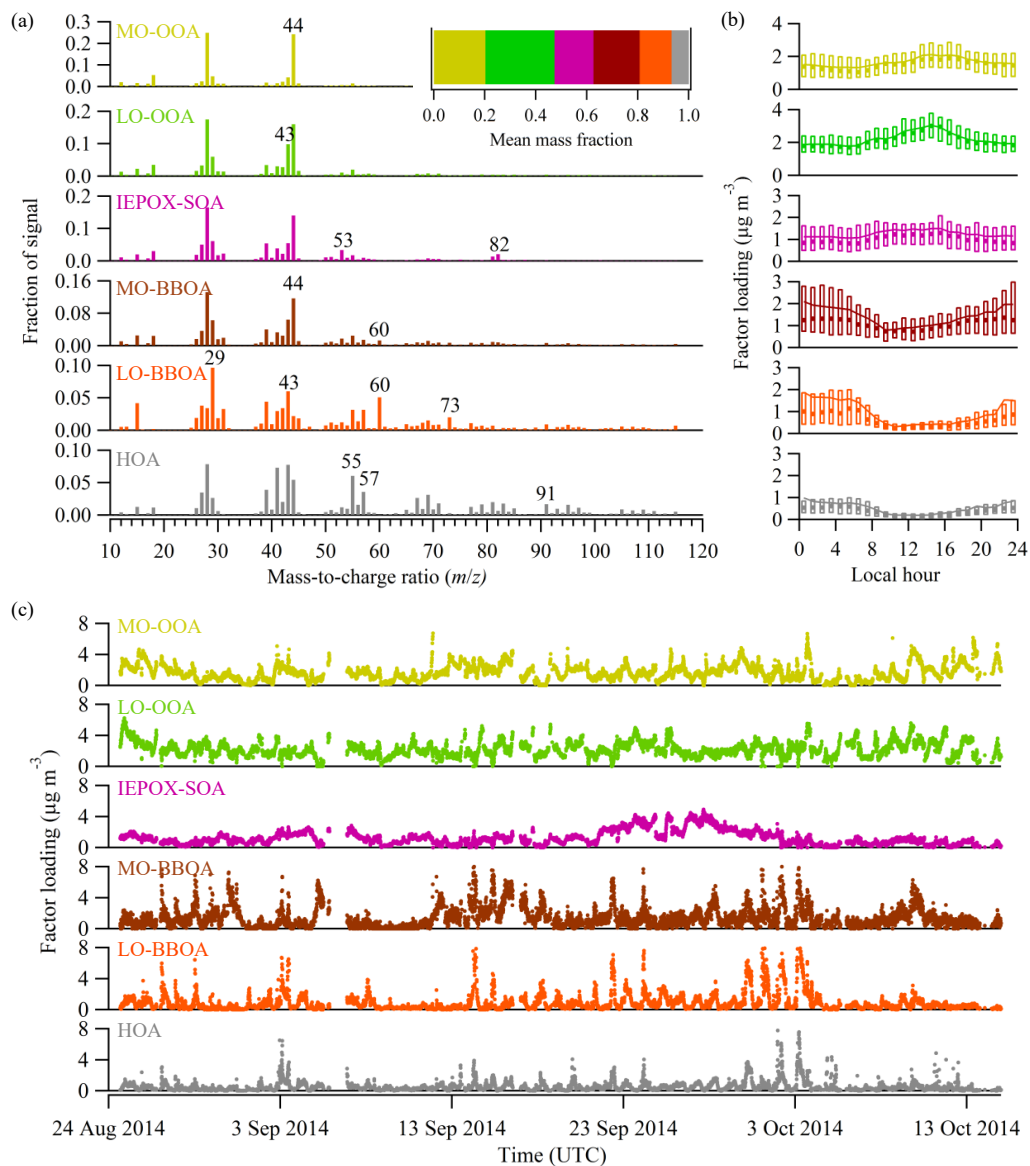


Figure 5

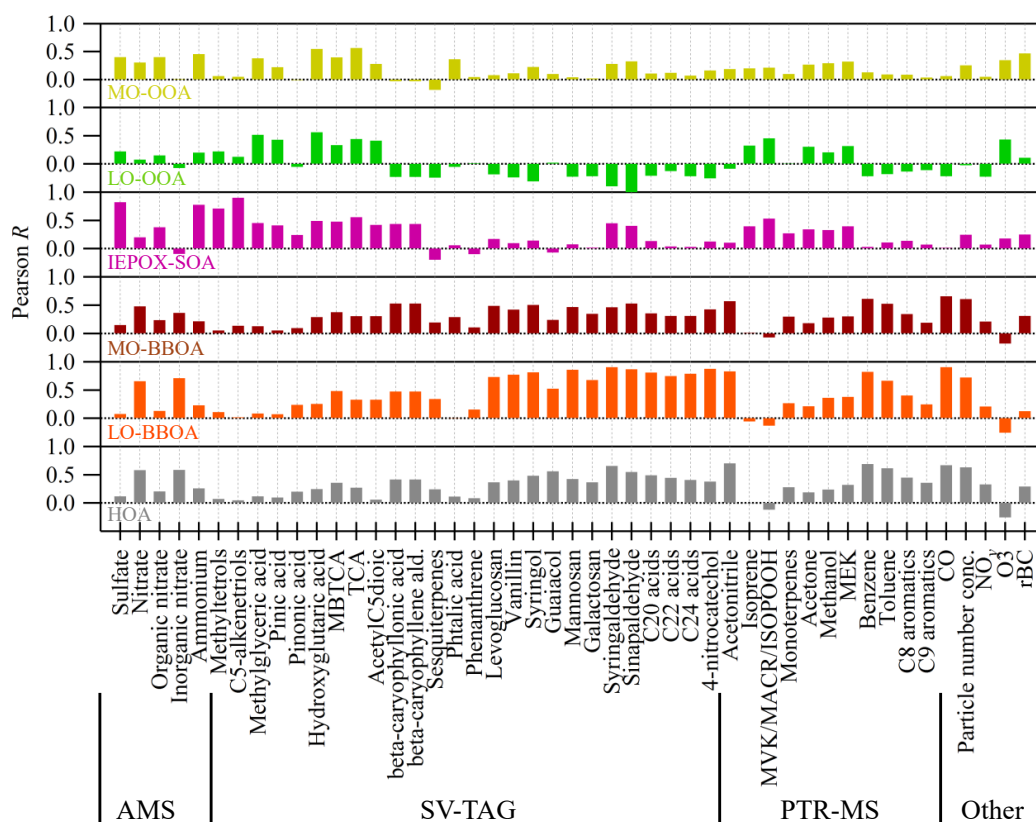


Figure 6

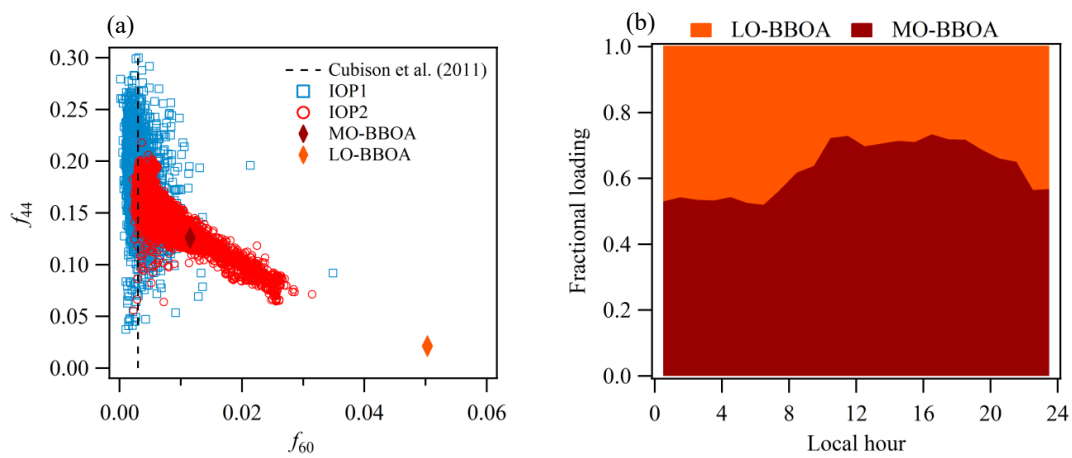


Figure 7

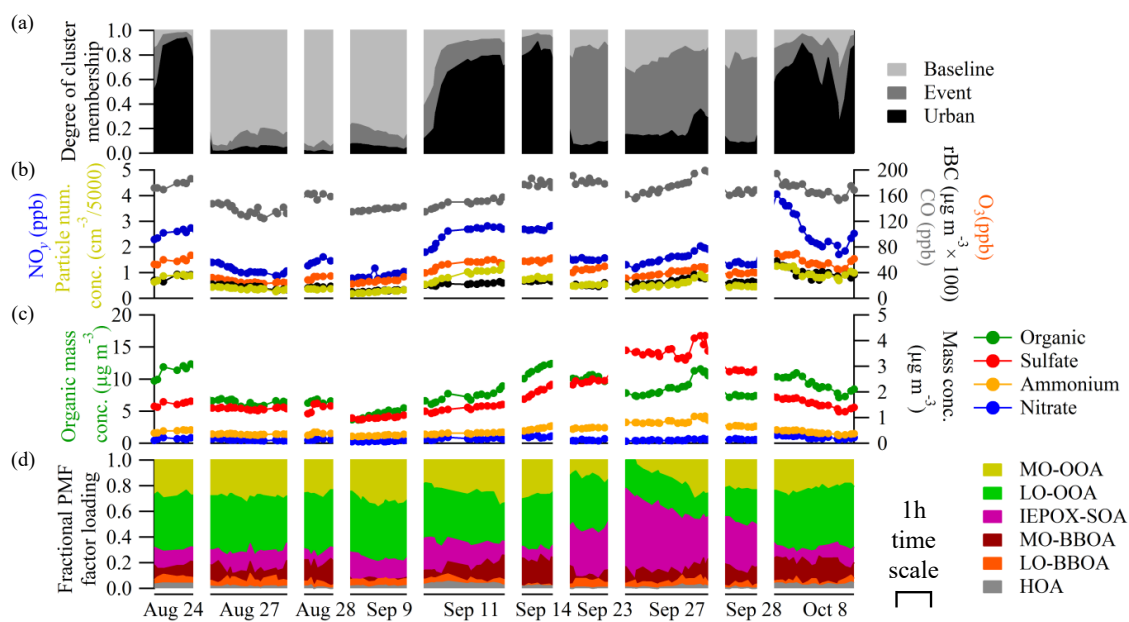


Figure 8

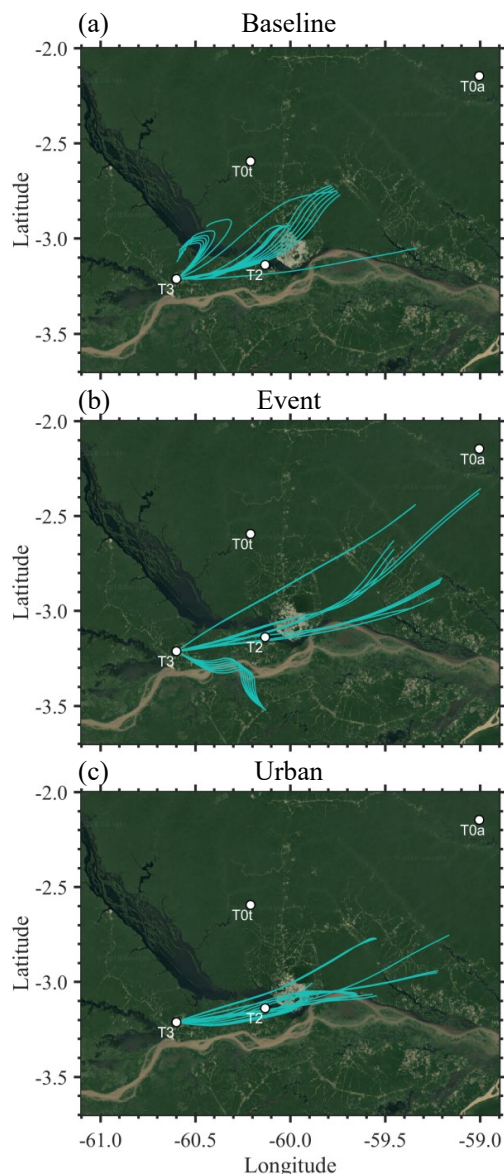


Figure 9

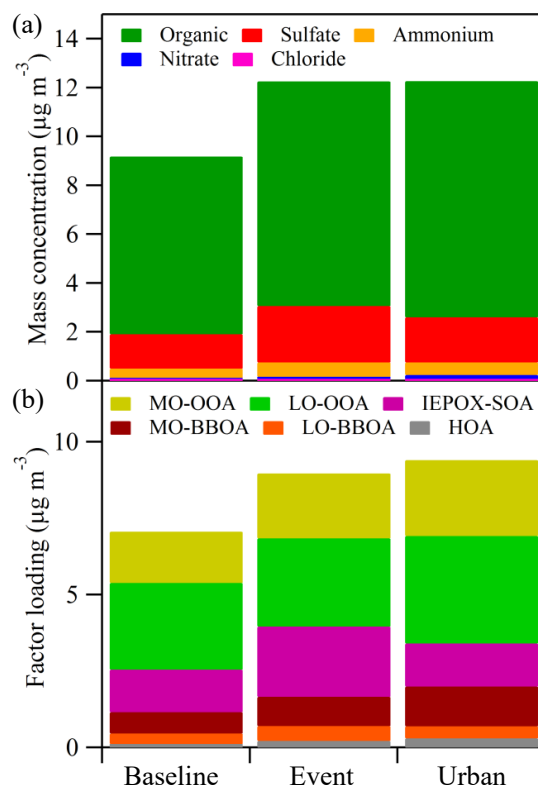


Figure 10



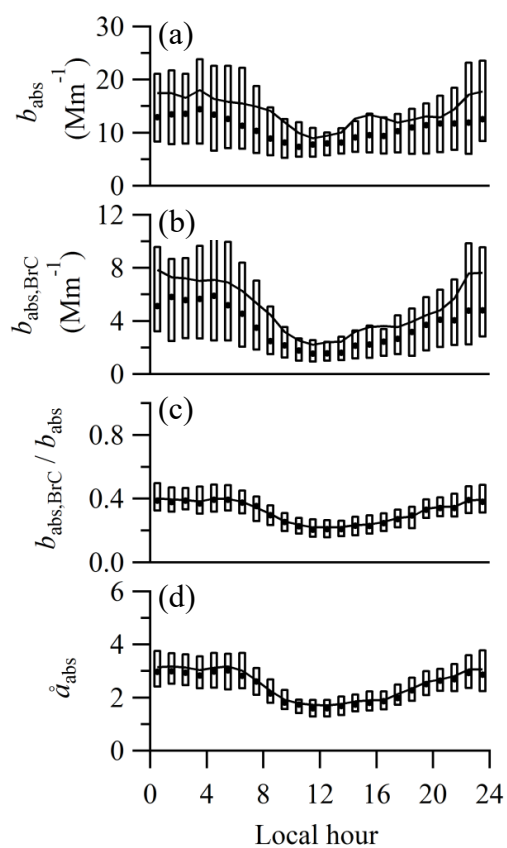


Figure 11

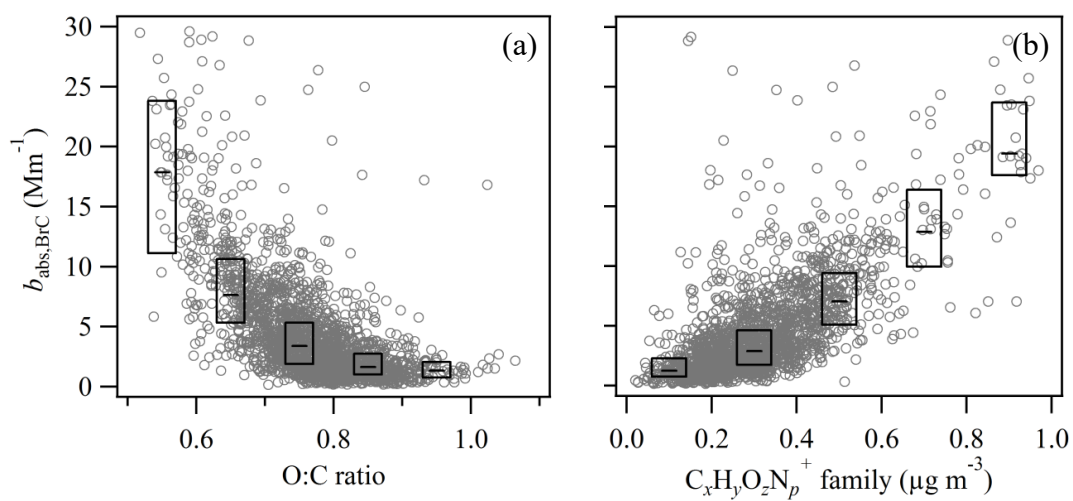


Figure 12

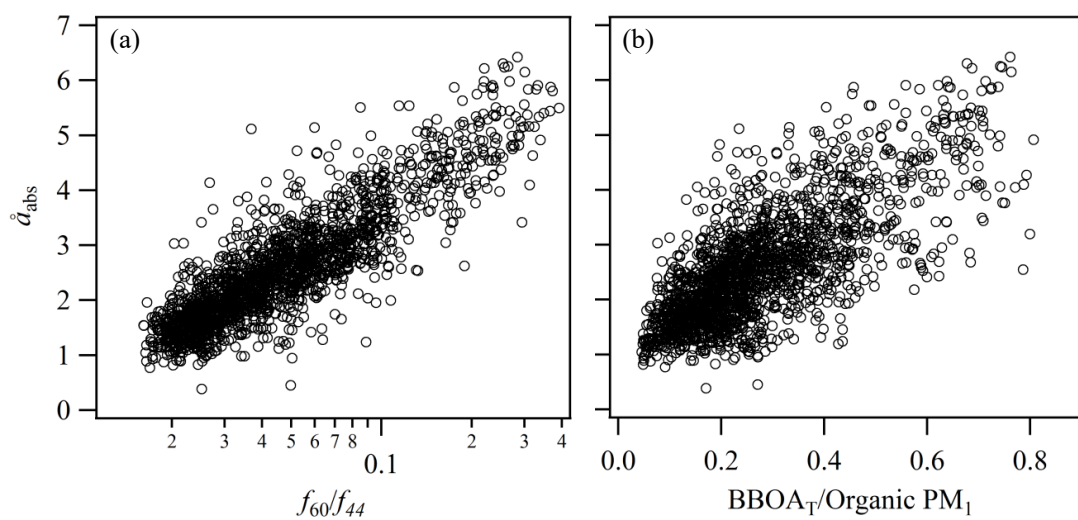


Figure 13

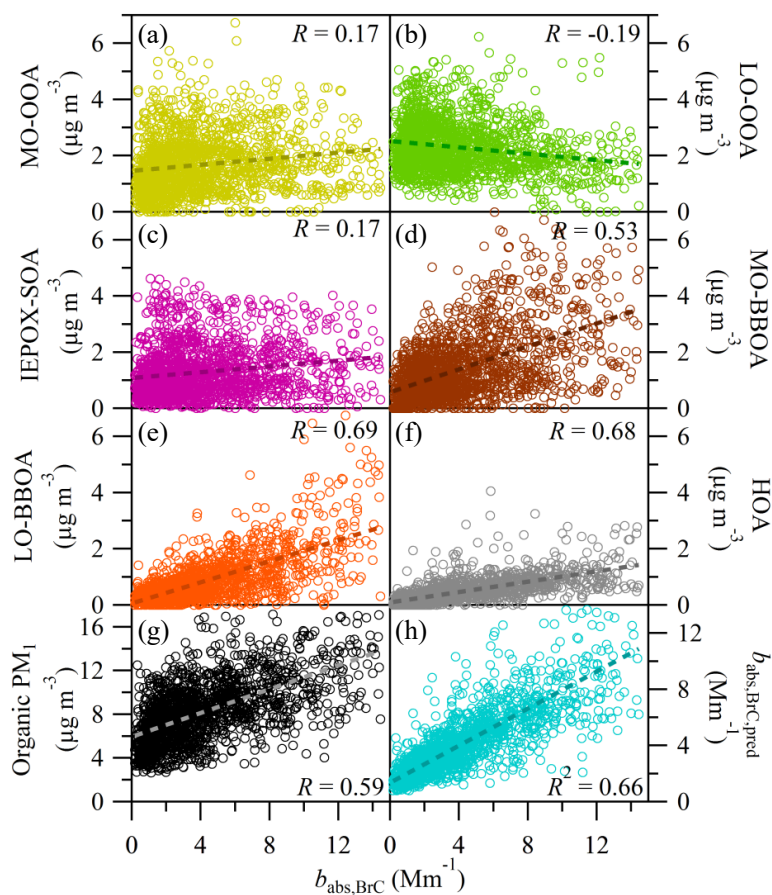


Figure 14

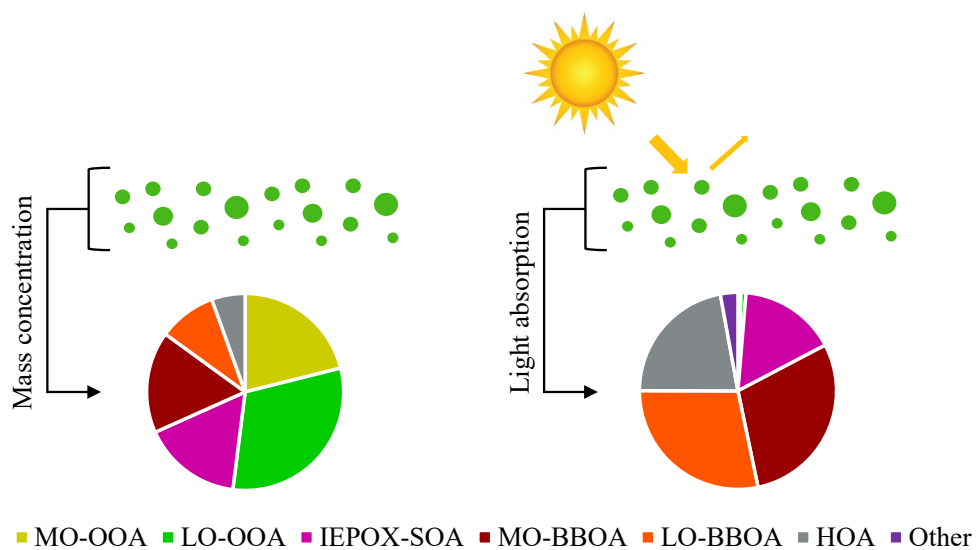


Figure 15